

Title	Lymph nodes harbor viral reservoirs that cause rebound of plasma viremia in SIV-infected macaques upon cessation of combined antiretroviral therapy.
Author(s)	Horiike, Mariko; Iwami, Shingo; Kodama, Makoto; Sato, Akihiko; Watanabe, Yuji; Yasui, Mika; Ishida, Yuki; Kobayashi, Takeshi; Miura, Tomoyuki; Igarashi, Tatsuhiko
Citation	Virology (2012), 423(2): 107-118
Issue Date	2012-02-20
URL	<a href="http://hdl.handle.net/2433/153287">http://hdl.handle.net/2433/153287</a>
Right	© 2011 Elsevier B.V.
Type	Journal Article
Textversion	author

1        **Lymph nodes harbor viral reservoirs that cause rebound of plasma**  
2        **viremia in SIV-infected macaques upon cessation of combined**  
3        **antiretroviral therapy**

4  
5  
6  
7        Mariko Horiike<sup>1</sup>, Shingo Iwami<sup>1,2,3</sup>, Makoto Kodama<sup>4</sup>, Akihiko Sato<sup>4</sup>, Yuji Watanabe<sup>1</sup>, Mika  
8        Yasui<sup>1</sup>, Yuki Ishida<sup>1</sup>, Takeshi Kobayashi<sup>1</sup>, Tomoyuki Miura<sup>1</sup> and Tatsuhiko Igarashi<sup>1#</sup>

9  
10  
11  
12  
13        <sup>1</sup>Laboratory of Primate Model, Experimental Research Center for Infectious Diseases, Institute  
14        for Virus Research, Kyoto University, Kyoto 606-8507, Japan, <sup>2</sup>Precursory Research for  
15        Embryonic Science and Technology (PRESTO), Japan Science and Technology Agency (JST),  
16        Kawaguchi, Saitama 332-0012, Japan, <sup>3</sup>Graduate School of Mathematical Sciences, The  
17        University of Tokyo, Meguro-ku, Tokyo 153-8914, Japan, and <sup>4</sup>Medical Research Laboratories,  
18        Shionogi & Co. Ltd., Osaka 566-0022, Japan.

19  
20  
21  
22  
23  
24  
25  
26        #Corresponding author:

27        Room 301

28        Molecular Biology Research Bldg

29        Institute for Virus Research

30        Kyoto University

31        53 Kawahara-cho, Shogoin,

32        Sakyo ward

33        Kyoto, Kyoto 606-8507, Japan

34        +81 75-751-3982 (Ph)

35        +81 75-761-9335 (Fax)

36        [tigarash@virus.kyoto-u.ac.jp](mailto:tigarash@virus.kyoto-u.ac.jp) (e-mail)

1  
2  
3  
4  
5  
6  
7  
8  
9  
10  
11  
12  
13  
14  
15  
16  
17  
18  
19  
20  
21  
22  
23  
24

**ABSTRACT**

Attempts to find a cure for HIV infection are hindered by the presence of viral reservoirs that resist highly active antiretroviral therapy. To identify the properties of these reservoirs, four SIV239-infected Rhesus macaques were treated with combined antiretroviral therapy (cART) for 1 year. While plasma viral RNA (vRNA) was effectively suppressed, a systemic analysis revealed that vRNA was distributed in the following order: lymphatic tissues > lungs and intestine > other tissues. Histochemistry yielded no cells with viral signals. To increase the chance of detection, two additional SIV-infected animals were treated and analyzed on Day 10 after the cessation of cART. These animals exhibited similar vRNA distribution patterns to the former animals, and immunohistochemistry revealed Nef-positive T lymphocytes predominantly in the follicles of mesenteric lymph nodes (MLNs). These data suggest that lymphatic tissues, including MLNs, contain major cellular reservoirs that cause rebound of plasma viremia upon cessation of therapy.

**KEYWORDS**

SIV, antiretroviral therapy, HIV-1, HAART, rebound of plasma viremia, reservoirs, animal model.

1  
2 **INTRODUCTION**  
3

4           Highly active antiretroviral therapy (HAART), which consists of three or  
5 more anti-HIV-1 drugs, is currently the primary choice of therapeutic intervention for  
6 HIV-1-infected individuals  
7 (<http://aidsinfo.nih.gov/contentfiles/AdultandAdolescentGL.pdf>). The circulating viral  
8 loads in these patients are, in most cases, effectively suppressed below the limit of  
9 detection (<50 copies/ml of plasma) by HAART (Richman, 2001). However, the virus  
10 loads promptly rebound to pretreatment levels upon cessation of HAART (Chun et al.,  
11 1999), which suggests the persistence of viral reservoirs during the combined antiviral  
12 therapy. Therefore, to achieve a complete cure of HIV-1 infection, it is essential to  
13 eradicate these viral reservoirs.

14           Resting CD4<sup>+</sup> T lymphocytes have been identified as a viral reservoir (Chun  
15 et al., 1997; Finzi et al., 1997; Wong et al., 1997). These cells harbor intact viral  
16 genomes integrated into their chromosomes and produce infectious virus particles when  
17 they are reactivated in response to stimulation. It is noteworthy that the estimated  
18 half-life of a resting CD4<sup>+</sup> T cell is more than 44 months (Siliciano et al., 2003), which  
19 provides a theoretical basis for the source of the virus that rebounds upon cessation of  
20 long-term, successful HAART. Resting CD4<sup>+</sup> T lymphocyte are probably not the only  
21 reservoir of HIV-1. In the majority of patients on HAART, the rebounding viral  
22 genotypes detected in the plasma upon cessation of therapy were dissimilar to the  
23 genotypes extracted from resting CD4<sup>+</sup> T cells or from virus particles recovered from  
24 cells that were collected before interruption of the therapy (Chun et al., 2000).

25           Follicular dendritic cells (FDCs) have also been proposed as a viral reservoir  
26 (Spiegel et al., 1992). These cells are present in the follicles formed in all secondary  
27 lymphoid tissue. Rather than being infected with virus, FDCs retain infectious HIV-1  
28 particles on the cell surface and transfer them to CD4<sup>+</sup> T lymphocytes (Burton et al.,  
29 2002). Since FDCs retain numerous virus particles, the genomes of which exhibit  
30 greater diversity than those in other tissues or cells and which reportedly hold infectious  
31 particles for months to years, it seems likely that these cells serve as archives of  
32 infectious virions (Keele et al., 2008).

33           The recently developed method for ultrasensitive detection of plasma viral

1 burdens has revealed that patients who have HAART-controlled viremia (below the  
2 detection limit by clinical criteria; i.e., <50 copies/ml plasma) over several years still  
3 harbor minuscule amounts of virion-associated RNA in the circulation (Palmer et al.,  
4 2008), suggesting ongoing viral replication, i.e., “residual viremia”. The potential for  
5 ongoing HIV-1 replication during HAART is supported by evidence of *env* gene  
6 evolution in patients receiving HAART (Frost et al., 2001; Martinez et al., 1999), as  
7 well as the detection in patients on HAART of 1-LTR and 2-LTR circles, episomal  
8 HIV-1 cDNAs, the presence of which most likely reflects recent infection (Sharkey et  
9 al., 2005; Sharkey et al., 2000). A transient increase in the number of 2-LTR circles,  
10 probably reflecting an increase in the number of failed attempts to integrate into the host  
11 cell genome, was detected in approximately 30% of infected individuals who were  
12 receiving HAART, when an integrase inhibitor was added as treatment intensification  
13 (Buzon et al., 2010). Based on these lines of evidence, it is conceivable that certain cell  
14 types, as yet to be identified, allow productive replication of HIV-1 during HAART.  
15 Although HAART theoretically arrests *de novo* virus replication, these unidentified  
16 reservoirs appear to be refractory to the antiviral effects of the regimen through  
17 unknown mechanisms.

18 It is postulated that viral reservoirs in the host retain HIV-1 during HAART as  
19 follows: resting CD4<sup>+</sup> T lymphocytes store inducible viral genomes, FDCs archive  
20 infectious particles, and unidentified cells support productive viral replication cycles. It  
21 remains to be revealed whether other cell types serve as viral reservoirs using other  
22 mechanisms, and which cell type is the most important for sequestering HIV-1.

23 Peripheral blood samples from volunteer patients have been used in studies to  
24 identify HIV-1 reservoirs (Brennan et al., 2009; Chun et al., 2000; Sharkey et al., 2011).  
25 However, HIV-1 predominantly replicates in CD4<sup>+</sup> T lymphocytes in the lymphoid  
26 tissues (Embretson et al., 1993; Pantaleo et al., 1993), particularly the intestine, which is  
27 home to 70-90% of all lymphocytes in the body and which is severely affected during  
28 the acute phase of infection (Brenchley et al., 2004; Guadalupe et al., 2003),  
29 determining prognosis. Therefore a systemic analysis, in addition to existing studies on  
30 peripheral blood, would elucidate the mechanisms underlying rebound of plasma  
31 viremia upon discontinuation of HAART. Since it is unethical to collect various tissues  
32 from patients for analysis, an alternative model system is required. In this regard, the  
33 SIV/macaque model, which has been useful in understanding HIV-1 infection, is

1 suitable for investigations of viral reservoirs using a systemic analysis (Dinoso et al.,  
2 2009; North et al., 2009).

3           Using the SIV239/macaque system, we investigated HIV-1 reservoirs during  
4           combined antiviral therapy (cART). First, we conducted a systemic analysis of  
5           SIV-infected Rhesus macaques that received cART for an extended period. SIV239 has  
6           been extensively used as a tractable animal model for HIV-1 in studies of replication,  
7           pathogenesis, and vaccine development. In addition, this virus causes almost complete  
8           depletion of CD4<sup>+</sup> T lymphocytes in the intestine (Veazey et al., 1998), as HIV-1 does in  
9           patients who suffer from AIDS.

## RESULTS

### Establishment of anti-SIV239 cART regimen with oral administration

Before the experimental infection of macaques with SIV, we established an antiretroviral regimen that is applicable to SIV239 infection in the Rhesus macaque model. Given that NNRTIs do not suppress replication of SIV (Balzarini et al., 1995), anti-HIV-1 drugs belonging to this class were excluded from consideration. Regarding NRTIs, several studies have confirmed that Tenofovir (TDF) and its pro-drug PMPA are effective against SIV. Some studies have used Zidovudine (AZT) and Lamivudine (3TC) to suppress SIV replication *in vitro* and *in vivo* (Balzarini et al., 1995; Benlhassan-Chahour et al., 2003). Based on the results of these studies, we included TDF (Viread) and AZT/3TC (Combivir) in our regimen. Regarding protease inhibitors (PIs), Saquinavir (SQV) has been shown to be effective against SIV *in vitro* (Giuffre et al., 2003; Witvrouw et al., 2004). When we initiated this study, the anti-SIV efficacies of other commercially available PIs had not yet been reported. To determine which PI to include in our cART, we examined three commercially available PIs—SQV, Lopinavir/Ritonavir (LPV/RTV; Kaletra), and Atazanavir (ATV; Reyataz)—in the MT-4/MTT assay. This assay, which was originally developed to measure cell proliferation, was used to evaluate inhibition of virus-induced killing of human T-lymphoid MT-4 cells in the presence of increasing amounts of the drugs (Pauwels et al., 1988). Along with SIV239, HIV-1 IIIB was employed in the assay as a control. All of the compounds tested suppressed the activity of SIV239. The EC<sub>50</sub> values for SQV were 18.5 nM against SIV and 22.7 nM against HIV-1 (Table 1 and Supplemental Figure 1). The EC<sub>50</sub> ratio, i.e., the EC<sub>50</sub> value against SIV divided by the EC<sub>50</sub> value against HIV-1, was 0.8 (Table 1). The EC<sub>50</sub>s against SIV239 and the EC<sub>50</sub> ratios of the other two drugs were: 52.2 nM and 1.5, respectively, for LPV/RTV; and 80.0 nM and 4.7, respectively, for ATV. Pharmacokinetic information on these drugs is available, and the half-life in the circulation in humans is: 1–2 h for SQV; 5–6 h for LPV/RTV; and 7 h for ATV (<http://aidsinfo.nih.gov/contentfiles/AdultandAdolescentGL.pdf>). Taking into account the EC<sub>50</sub>, the half-life (which defines the required frequency of administration to maintain the drug level), and cost-effectiveness, we included LPV/RTV in our regimen.

Drug administration was instituted *per os*, to effectively model the metabolism and pharmacokinetics of the antiviral drugs in patients. The dosage and

1 administration of these drugs are described in the *Materials and Methods* section. To  
2 assess whether a given dosage resulted in a measurable concentration of the drug in the  
3 circulation even after a long interval, blood samples were collected from six monkeys at  
4 14 h after intake and the antiviral effect in plasma was determined by titration. The drug  
5 concentrations in the animals' blood ranged from 7.2–29.5  $\mu\text{M}$  (LPV/RTV equivalent);  
6 these levels are 5- to 20-fold higher than those recommended for adult patients  
7 (1.5  $\mu\text{M}$  for LPV/RTV equivalent)  
8 (<http://aidsinfo.nih.gov/contentfiles/AdultandAdolescentGL.pdf>). Plasma samples from  
9 two representative animals, which had already been measured in the biological assay,  
10 were also subjected to HPLC. The results of the HPLC analysis revealed drug  
11 concentrations comparable to those determined by the biological assay: 16.1  $\mu\text{M}$  for one  
12 animal (20.0  $\mu\text{M}$  by the MTT assay) and 25.7  $\mu\text{M}$  for the other animal (24.8  $\mu\text{M}$  by the  
13 MTT assay), thus justifying our use of the biological assay to measure levels of antiviral  
14 activity in the circulation of SIV-infected animals during therapy. Based on these results,  
15 we finalized the regimen.

16

### 17 **Efficacy of the cART regimen for macaques infected with SIV239**

18 The establishment of the anti-SIV regimen enabled us to conduct animal  
19 experiments. Seven Rhesus macaques were inoculated intravenously with 2,000 TCID<sub>50</sub>  
20 of the SIV239 virus stock. All animals exhibited an initial peak of viremia at 2 weeks  
21 post-inoculation (pi) (median,  $2.2 \times 10^7$  copies/ml; range,  $7.9\text{--}60.0 \times 10^6$  copies/ml,  
22 Figure 1). At 8 weeks pi, when the viral loads decreased from the initial peak and  
23 plateaued (median,  $1.3 \times 10^5$  copies/ml; range,  $1.1\text{--}4.9 \times 10^5$  copies/ml), the cART was  
24 administered to four of the monkeys (MM491, MM499, MM528, and MM530;  
25 designated as group A).

26 Upon drug administration, the plasma viral RNA (vRNA) levels in these animals  
27 promptly started to decrease. There was an inverse inclination between set point plasma  
28 vRNA load and duration to suppress vRNA to the detection limit (200 copies/ml). The  
29 vRNA of MM491, whose set point viral RNA level was the lowest in the group  $1.1 \times 10^5$   
30 copies/ml, fell below the detection limit in 2 weeks. MM499 and MM528, whose  
31 plasma vRNAs were  $4.4 \times 10^5$  and  $1.3 \times 10^6$  copies/ml at the initiation of cART, took 5  
32 and 6 weeks, respectively. After nine weeks of treatment, the viral burden of MM530,  
33 which had the highest level in the group at  $4.9 \times 10^6$  copies/ml, was undetectable. Plasma



1 vRNA levels of all animals on cART had fallen below the limit of detection by 17  
2 weeks pi. When HAART was applied to SIV/pigtailed macaque or RT-SHIV/rhesus  
3 macaque models, it took 8 and 18 weeks, respectively, to suppress circulating vRNA to  
4 below the detection limit (Dinoso et al., 2009; North et al., 2009). When considering  
5 variables from previous studies, including virus strain, drug combinations, detection  
6 limit of vRNA measurement, and initiation of treatment of these studies, it is  
7 conceivable that the cART approach devised in the current study is as potent in terms of  
8 the progress to viral containment.

9 To relate our results to previous studies on vRNA declines for HIV-1 and SIV  
10 following antiviral therapy, we examined the levels of viremia in our infected monkeys  
11 during the first few weeks after the initiation of therapy (Table 2 and Supplemental  
12 Figure 2). Each individual monkey followed a similar pattern of viral decay: an initial  
13 rapid and exponential reduction by almost 2.5 orders of magnitude (comprising the first  
14 phase, which is presumably associated with short-lived infected cells), followed by a  
15 slower exponential decline of 1.5 orders of magnitude (the second phase, which is  
16 presumably associated with long-lived infected cells). The observed biphasic decay of  
17 viral burdens was consistent with previous findings from studies on SIV models and  
18 patients with HIV-1 (Dinoso et al., 2009; Murray et al., 2007; Perelson et al., 1997;  
19 Perelson and Nelson, 1999). Decay rates for the first and second phases were deduced  
20 by employing mathematical modeling (Table 2). The decay rates of the first phase  
21 ranged from 0.495 (for MM491) to 0.853 (for MM499), and those of the second phase  
22 ranged from 0.028 (for MM491) to 0.089 (for MM499). The decay rates of plasma  
23 vRNA loads during the first phase in patients with HIV-1 on HAART, consisting of  
24 LPV/RTV, Efavirenz, 3TC, and TDF, exhibited comparable numbers to those in the  
25 current study, ranging from 0.6 to 1.4 (Markowitz et al., 2003). Mean half-lives of  
26 ( $\log_2/a =$ ) 1.13 for the first phase and ( $\log_2/\mu_M =$ ) 14.24 days for the second phase

27 were comparable to those observed in patients with HIV-1 on HAART. Half-lives of  
28 HIV-1 RNA in the circulation of HIV-1-infected patients on suppressive ART, consisting  
29 of Indinavir and Efavirenz, ranged from 0.6 to 2.0 days for the first phase and 5.2 to  
30 35.6 days for the second phase (Havlir et al., 2003). Comparison of the viral decay rates  
31 derived in the current study with those derived in previous reports (Perelson et al.,  
32 1997) gave statistically insignificant results ( $P = 0.667$  for the first phase, and  $P = 0.662$

1 for the second phase). These results suggest that the virologic response of SIV infected  
2 Rhesus macaques to cART, as reported in a recent study (Dinoso et al., 2009), is  
3 comparable to the response of HIV-1-infected patients to HAART.

4 Patients with HIV-1 on HAART exhibit undetectable levels of plasma vRNA  
5 (typically less than 50 copies/ml) when the therapy works as expected. To estimate  
6 suppression levels achieved by the regimen used in the current study, selected plasma  
7 samples with adequate volume from animals in group A were subjected to another  
8 quantitative real-time PCR assay with a lower detection limit. Using 1.5-ml plasma  
9 samples, which were collected at 29, 42, and 52 weeks pi, and at euthanasia,  
10 particle-associated vRNA was extracted and amplified. All of these samples yielded less  
11 than 20 copies/ml of vRNA loads (Table 3), except for those collected at 42 and 52  
12 weeks pi (44 and 47 copies/ml, respectively) from MM530, which exhibited the highest  
13 plasma vRNA at the start of cART ( $4.9 \times 10^6$  copies/ml) and required the longest  
14 duration to suppress vRNA to 200 copies/ml (9 weeks). These results confirm that the  
15 regimen established in the current study is as suppressive as those applied to patients.  
16 Based on the progression to viral containment, decay rates, and suppression levels, we  
17 concluded that the cART established in the current study is comparable to therapies  
18 used to treat patients with HIV-1 and suitable to pursue viral reservoirs during therapy.  
19 The suppressed viral burdens of the treated animals were maintained below the limit of  
20 detection throughout the course of treatment (up to 52 weeks). In contrast, the viral  
21 burdens of the untreated animals (MM496, MM510, and MM521) remained at  $>1.0 \times$   
22  $10^5$  copies/ml until the day of necropsy (Figure 1). Assuming a limit of viral detection  
23 of 200 copies/ml, there was a statistically significant difference in the plasma vRNA  
24 levels between the two groups of animals at Week 42 ( $P < 0.05$ ).

25 During the entire course of cART, the levels of antiviral activity in the plasma  
26 samples of animals MM491, MM528, and MM530 assessed by MT-4/MTT assay were  
27 above the recommended trough level for adult patients (for MM491: range, 3.5–17.8  
28  $\mu\text{M}$  LPV/RTV equivalent; for MM528: range, 6.0–24.9  $\mu\text{M}$  LPV/RTV equivalent; for  
29 MM530: range, 8.2–14.2  $\mu\text{M}$  LPV/RTV equivalent) (Table 4). Even in the remaining  
30 animal, MM499, in which the circulating concentration of the activity was below the  
31 recommended trough level at the two time-points tested, at 10 weeks pi and at autopsy,  
32 during the course of antiviral therapy, the plasma vRNA levels were below the limit of  
33 detection. None of the treated animals exhibited a transient surge in vRNA level during

1 the entire course of the therapy. Certain clinical conditions are known to be side-effects  
2 of antiviral drug treatment  
3 (<http://aidsinfo.nih.gov/contentfiles/AdultandAdolescentGL.pdf>). Among the drugs  
4 employed in the present study, TDF potentially causes renal complications (Van  
5 Rompay et al., 2004) and LPV/RTV can induce abnormal lipid metabolism. In general,  
6 no significant adverse effects were noted for the drugs employed in the present study.  
7 We conclude that the antiretroviral therapy regimen established in the current study is as  
8 effective as the combined antiretroviral therapy applied to patients with HIV.

### 9 10 **Higher titers of vRNA were detected in the lymphoid tissues of virus-infected** 11 **animals undergoing antiretroviral therapy**

12 The establishment of an effective antiretroviral therapy regimen for  
13 SIV-infected monkeys was a prerequisite for the identification of virus reservoirs during  
14 combined antiviral therapy. To this end, we considered two important questions: ‘Is  
15 virus replication maintained during the therapy?’, and ‘If active virus replication  
16 persists, are there particular anatomic compartments that allow preferential virus  
17 replication?’

18 To answer these questions, we looked for the presence of vRNA in a variety  
19 of tissues collected from animals receiving cART over a period of 1 year. Total RNA  
20 was extracted from each tissue and subjected to real-time reverse transcription  
21 (RT)-PCR. Table 5 summarizes the results of RT-PCR for four animals in group A that  
22 were subjected to analysis at the end of the 1-year cART regimen, along with a  
23 representative animal that was not given treatment (MM521); all the animals were  
24 euthanized at between 61 and 68 weeks pi. In the untreated monkey (MM521), vRNA  
25 was detected in all the tissues examined, with the exception of the brainstem. In the  
26 lymphoid tissues, higher titers of vRNA (approximately  $1.0 \times 10^8$  copies/ $\mu$ g total RNA)  
27 were detected. In the gastrointestinal tract, lungs, and vagina, in which the resident  
28  $CD4^+$  T-lymphocyte population consists mainly of  $CCR5^+$  memory cells (the preferred  
29 target of HIV-1 and SIV) (Douek et al., 2003; Meng et al., 2000; Veazey et al., 2000),  
30 the vRNA titers were approximately  $1.0 \times 10^6$  copies/ $\mu$ g of total RNA. Lower levels of  
31 vRNA were detected in the non-lymphoid tissues (heart, liver, and kidneys) and the  
32 central nervous system (cerebrum and cerebellum).

33 In the group A macaques, the vRNA titers in several tissues were much lower

1 than those found in the untreated animals. The non-lymphoid tissues and central  
2 nervous system did not contain measurable amounts of vRNA. Low levels of vRNA  
3 were detected in the effector sites, such as the intestine (up to  $6.5 \times 10^4$  copies/ $\mu\text{g}$  total  
4 RNA), lungs, and vagina (up to  $6.5 \times 10^3$  copies/ $\mu\text{g}$  total RNA). Statistical analysis of  
5 vRNA burdens revealed significant reductions in the jejunum and rectum of animals in  
6 group A as compared to those of untreated controls ( $p = 0.03$ ), indicating that cART  
7 suppressed vRNA expression in those tissues, although incompletely. Compared to the  
8 above-mentioned tissues, higher levels of vRNA (approximately  $1.0 \times 10^5$  copies/ $\mu\text{g}$  of  
9 total RNA) were detected in the lymphoid tissues. Of note, both the superior and  
10 inferior mesenteric lymph nodes (sMLNs and iMLNs, respectively) were among the  
11 tissues that contained the highest titers of vRNA in animals on cART. Statistical analysis  
12 of vRNA in the lymphatic tissues also revealed significant suppression in group A as  
13 compared to controls (iliac and submandibular lymph nodes and iMLNs,  $p = 0.03$ ).

14 To identify the cell type(s) that support vRNA synthesis and, potentially,  
15 allow viral proteins to be produced during ART, we prepared tissue sections from the  
16 animals in group A and subjected them to *in situ* hybridization (ISH) and  
17 immunohistochemistry (IHC). While these tissues yielded no positive signals, the same  
18 staining techniques detected vRNA-positive cells and viral-protein-positive cells in  
19 tissue sections prepared from untreated animals (data not shown).

20 In summary, our initial questions were resolved as follows: the presence of  
21 vRNA in the gut, lungs, vagina, and lymphoid tissues indicated active viral replication  
22 in animals that were treated with cART for 1 year, and the lymphatic tissues allowed  
23 preferential viral replication in these animals.

24

## 25 **SIV Nef-producing T lymphocytes predominated in the follicles of the MLNs from** 26 **an animal that exhibited rebound of plasma viremia upon cessation of cART**

27 Quantitative PCR analysis of vRNA in a variety of tissues collected from  
28 SIV-infected animals that were on prolonged chemotherapy (i.e., the animals in group  
29 A) indicated that the lymphatic tissues acted as the anatomic compartment for active

1 virus replication during antiretroviral therapy. However, we were unable to identify  
2 histochemically any vRNA-positive or viral-protein-positive cells in the tissue sections  
3 prepared from these animals. This discrepancy was likely due to the lower sensitivity of  
4 these staining techniques as compared to PCR. We assumed that cessation of ART  
5 would result in rebound of plasma viremia, thereby promoting the transcription and  
6 translation of viral genes to levels detectable by the histochemical staining techniques  
7 employed in the present study. Based on this assumption, we took advantage of the  
8 rebound of plasma viremia as a surrogate approach to identify the viral reservoir(s)  
9 during cART. Thus, two Rhesus macaques (MM508 and MM511, designated as group  
10 B animals) were inoculated with the same SIV239 virus stock as was used to inoculate  
11 the group A animals. The group B animals exhibited an initial peak of viremia at  
12 2 weeks pi (range,  $7.7\text{-}8.4\times 10^7$  copies/ml; Table 6), and the viral loads decreased and  
13 stabilized from 8 wpi onwards. Upon initiation of cART at 38 wpi, the levels of virus  
14 decreased rapidly and eventually fell below the limit of detection. The suppressed viral  
15 burdens were maintained until cessation of the treatment at 46 weeks pi. We attempted  
16 to determine the time-point at which the levels of viral gene transcription and translation  
17 were just above the detection limit of our staining. Since we envisioned that rebound of  
18 plasma viremia would take place within 2 weeks of interruption of therapy, animals  
19 were euthanized for necropsy on Day 10 after cessation of cART. The viral load in the  
20 plasma of animal MM511 was 1400 copies/ml, while that of animal MM508 was below  
21 the limit of detection (Table 6). Thus, one animal was exhibiting rebound of plasma  
22 viremia while the other animal had not yet reached that stage when they were killed for  
23 analysis.

24           The overall tendency of the vRNA distribution in the group B animals was  
25 similar to that observed in the group A animals, with the titers being somewhat higher  
26 in group B. Higher levels of vRNA ( $>1.0\times 10^4$  copies/ $\mu\text{g}$  total RNA) were detected  
27 exclusively in the lymphoid tissues (Table 7). In MM511, the highest level of vRNA  
28 was detected in the MLNs ( $>1.0\times 10^6$  copies/ $\mu\text{g}$  total RNA). MM508, in which the  
29 plasma viral load was below the limit of detection at euthanasia, contained high levels  
30 of vRNA ( $>1.0\times 10^5$  copies/ $\mu\text{g}$  of total RNA), but only in the spleen and iMLN.

31           Based on the increased levels of vRNA transcription, we hypothesized that  
32 higher levels of viral proteins were synthesized in these two animals (MM508 and  
33 MM511) than in the group A animals. We subjected all the lymphoid tissues collected

1 from these two animals to IHC, to identify viral-protein-producing cells. First, we  
2 focused on MM511, which exhibited higher viral titers in the plasma and lymphoid  
3 tissues than MM508, and stained tissue sections from this animal with anti-Nef  
4 antibodies. IHC yielded Nef-positive cells. The viral-protein-positive cells were mainly  
5 localized to the globular architecture in the lymph node cortex, most likely the  
6 lymphoid follicles, and the Nef-positive cells bore morphologic characteristics similar  
7 to those of T lymphocytes (Figure 2a). To clarify the architecture within which the  
8 Nef-producing cells were detected, we conducted combined IHC with an anti-Nef  
9 antibody (visualized with DAB) and an antibody directed against CD35 (visualized with  
10 VECTOR Blue). CD35 is a cell surface marker for FDCs, which are found exclusively  
11 in the follicles of the secondary lymphoid tissues. The combined staining showed that  
12 Nef-positive cells and FDCs were present in the same globular architecture, suggesting  
13 that the viral-protein-producing cells were predominantly located in the follicles of the  
14 lymph nodes of this animal. Moreover, staining revealed that the Nef-producing cells  
15 were juxtaposed on the FDCs (Figure 2b).

16 To confirm the identity of the viral-protein-expressing cells, we conducted  
17 combined immunofluorescence staining with an anti-Nef antibody (visualized with  
18 Alexa Fluor 488) and an anti-CD3 antibody (visualized with Alexa Fluor 594). After  
19 extensive observations of the stained sections under the microscope, we detected  
20 Nef-positive cells in 16/305 sections prepared from a variety of lymphatic tissues  
21 collected from animal MM511, and these viral-protein-expressing cells were all positive  
22 for CD3 (Figure 3 and Table 8). Of these 16 sections, 12 were prepared from MLNs and  
23 4 from other anatomical compartments. The viral-protein-producing cells in the follicles  
24 constituted around 75% of all the positive cells detected. In some sections, Nef-positive  
25 cells were clustered in the follicles (Figure 3c).

26 In animal MM508, which was subjected to analysis before rebound of plasma  
27 viremia had taken place, the staining revealed a single Nef-positive cell that was also  
28 positive for CD3 (data not shown). The frequency of positive cells in this animal was  
29 substantially lower (one positive cell in 136 sections) than that in MM511.

30 In summary, in the animal that exhibited rebound of plasma viremia after  
31 cessation of cART, almost all the viral-protein-synthesizing cells, presumably  
32 productively infected cells, that were detected in the MLNs were identified as T  
33 lymphocytes, most likely CD4<sup>+</sup> T cells. The vast majority of the virus-infected T cells

1 were observed in the lymphoid follicles during rebound of plasma viremia (Table 8).

2

1  
2 **DISCUSSION**

3 The presence in infected individuals of HIV-1 viral reservoirs that persist  
4 during HAART impedes curing and complete eradication of the virus. While studies  
5 have been conducted into the identity and properties of the HIV-1 reservoirs (Brennan et  
6 al., 2009; Chun et al., 2000; Sharkey et al., 2011), much remains to be learnt. We  
7 reasoned that systemic analyses of infected individuals who were undergoing intensive  
8 ART would advance the characterization of the viral reservoirs (Dinosa et al., 2009;  
9 North et al., 2009). Therefore, we analyzed SIV-infected Rhesus macaques that  
10 underwent cART for 1 year. The major finding of the current study is that lymphatic  
11 tissues, including MLNs, contained higher numbers of cellular virus reservoirs that  
12 potentially cause rebound of plasma viremia upon cessation of cART. This assertion is  
13 based on the following observations: the lymphatic tissues contained the highest levels  
14 of vRNA in all the animals, regardless of cART, and the viral-protein-expressing T cells  
15 were localized predominantly to the MLNs of the animal that exhibited rebound of  
16 plasma viremia after cessation of cART.

17 We finalized the drug dosages to be administered by monitoring plasma  
18 trough levels of antiviral activity at 14 h post-consumption. During this process we  
19 discovered that the drug metabolism of monkeys is somewhat higher than that of  
20 humans. To fine-tune the drug concentrations in the circulation, 50% of the dosage  
21 established in the present study, corresponding to 150% of the dosage for a 60-kg adult  
22 patient, was given to the same animals. The circulating drug concentration at 14 hours  
23 post-consumption yielded no measurable net antiviral activity (data not shown).  
24 Therefore, it is necessary to determine an appropriate dosage for each drug prior to  
25 administration to animals. In this regard, one of the monkeys in group A, MM499,  
26 exhibited fluctuating antiviral activity during the therapy. At 10 and 64 weeks pi, the  
27 antiviral activity in the blood were below the recommended trough level for patients  
28 (1.5  $\mu$ M) (Table 4). Despite the fluctuation of antiviral activity, the viral burden of this  
29 animal was maintained below the limit of detection during the therapy, and systemic  
30 analysis revealed levels of vRNA that were comparable to those detected in the other  
31 three animals in group A (Table 5). That the other three animals also exhibited  
32 fluctuating concentrations of the drug in the circulation underlines the importance of  
33 monitoring antiviral activity in circulation during therapy, to ensure that the



1 administration schedule produces the expected antiviral activity.

2 RT-PCR analyses revealed that lymphatic tissues contained higher titers of  
3 vRNA than the other tissues in 4/4 SIV-infected macaques in group A, and 2/2 animals  
4 in group B followed the same distribution of vRNA (Table 5 and 7). In SIV-infected  
5 monkeys treated with cART, the Lamivudine concentration was more than 300-fold  
6 higher in the gastrointestinal tract than in the peripheral lymph nodes (Bourry et al.,  
7 2010). The finding of Bourry et al. explains our observation that chemotherapy was  
8 more effective at suppressing virus replication in the intestine than in the lymph nodes.  
9 It is possible that lymphatic tissues serve as viral sanctuaries, especially when the  
10 amount of drug accumulated in the tissues is insufficient to suppress virus replication. It  
11 should be noted that while viral load and drug concentration in the plasma are easily  
12 monitored, they do not reflect precisely the virus replication/drug distribution in specific  
13 important anatomic compartments.

14 Our results are also in good agreement with the results reported by North et al.,  
15 who performed a thorough analysis of a variety of tissues collected from  
16 RT-SHIV-infected animals that were receiving combined anti-viral therapy (North et al.,  
17 2009). The authors employed RT-SHIV, which is a chimeric virus that carries the  
18 HIV-1-derived RT gene on the backbone of SIV239, to model HAART to patients, in  
19 the context of SIV, since non-nucleotide reverse-transcriptase inhibitors (NNRTIs), one  
20 of the core components of HAART, do not suppress reverse transcription mediated by  
21 SIV RT (Balzarini et al., 1995). Although the cART regimen devised in the current  
22 study is unlike the HAART administered to patients, especially with respect to the  
23 employment of certain drugs, the viral decay rate in the circulation (calculated based on  
24 a two-compartment model) is comparable to that observed in patients treated with the  
25 multi-drug regimen (Murray et al., 2007; Palmer et al., 2008; Perelson et al., 1997)  
26 (Table 2 and Supplemental Figure 2). Therefore, it is implied that the lymphatic tissues  
27 may harbor higher titers of vRNA in HIV-1-infected patients on HAART, despite the  
28 viral burdens in the circulation are clinically non-detectable. The caveat is that the  
29 animals in the current study were on treatment for up to 1 year only, which is a  
30 considerably shorter treatment period than that of patients who have achieved successful  
31 virus containment since the beginning of the HAART era. Given that the desired  
32 concentration of the drug may not be reached in the lymphatic tissues, it is necessary to  
33 devise a way to deliver in a preferential manner either antiviral drugs or a specific injury

1 to these compartments, in combination of HAART, to achieve eradication of the virus,  
2 which is a crucial step towards a complete cure for HIV-1 infection.

3 Histochemical analyses revealed that the SIV Nef protein was expressed in T  
4 lymphocytes predominantly resident in the follicles formed in the MLNs of animal  
5 MM511, which exhibited viral rebound after cessation of cART (Figure 3 and Table 8).  
6 Active virus replication in the follicles of lymph nodes has been described (Folkvord et  
7 al., 2005). Previous studies have suggested that lymphatic follicles serve as preferred  
8 sites of virus replication, probably *via* FDCs and sequestration of virus-infected cells  
9 from cytotoxic T lymphocytes (CTLs). FDCs, which may interact with CD4<sup>+</sup> cells  
10 within the “enclave”, retain infectious virus particles and produce TNF- $\alpha$ , which  
11 promotes HIV replication (Thacker et al., 2009). HIV-1-specific CTLs fail to  
12 accumulate within lymphoid follicles, allowing unchecked virus replication in this  
13 architecture (Connick et al., 2007). Taken together, these findings support our  
14 observations of active viral protein synthesis in the lymphoid follicles.

15 The present study does not identify definitively the viral reservoirs. However,  
16 it does not rule out any of the proposed candidate reservoirs: resting CD4<sup>+</sup> T  
17 lymphocytes, FDCs, and unidentified cells involved in ongoing virus replication during  
18 therapy. To place our results in the context of current thinking regarding putative viral  
19 reservoirs, we make the following important points:

20 North et al. detected proviral DNA in the resting CD4<sup>+</sup> T-lymphocyte fraction  
21 prepared from MLNs (North et al., 2009). Dinoso et al. recovered replication-competent  
22 viruses in the cell fraction (Dinosa et al., 2009). It is possible that the Nef-positive cells  
23 detected in the current study were reactivated upon stimulation, thereby prompting  
24 resumption of the virus replication cycle; the progeny viral particles from these cells  
25 would initiate multiple rounds of replication in the T cells of the paracortical area and  
26 the follicles of the lymph nodes.

27 We detected FDCs juxtaposed on the Nef protein-positive T lymphocytes.  
28 This observation is not definitive evidence that FDCs transmit infectious viral particles  
29 to CD4<sup>+</sup> T cells. Based on our observations, we hypothesize that FDCs transmit virus to  
30 CD4<sup>+</sup> T cells or stimulate infected cells, so as to initiate viral rebound. An important  
31 caveat is that the animal in question was treated for only 8 weeks. Since FDCs are  
32 known to retain virus particles with their infectivity intact for a certain period of time  
33 (Keele et al., 2008), it would be informative to determine whether the interaction

1 between these two cell types occurs in animals that exhibit rebound after a prolonged  
2 period of therapy, followed by cessation.

3           Although we have no direct evidence that unknown cells are involved in  
4 ongoing viral replication during therapy, higher titers of vRNA were detected in the  
5 lymphatic tissues, primarily the MLNs, which suggests that certain cell types in this  
6 compartment allow viral replication during chemotherapy. It is likely that the levels of  
7 transcription of viral genes and of subsequent translation are too low to be detected by  
8 the staining techniques employed in the current study.

9           Based on our results, we postulate the following sequence of events after the  
10 cessation of HAART in individuals infected with HIV-1: in the follicles of the lymph  
11 nodes, such as MLNs, viruses that are preserved in certain forms, such as intact  
12 genomes and infectious particles, and with low-level ongoing replication, resume a  
13 productive replication cycle, preceding other anatomical compartments, when the  
14 concentration of the antiviral drug declines due to discontinuation of therapy; thereafter,  
15 other anatomic compartments resume productive viral replication owing to weakened  
16 containment of the virus and higher accumulations of the drugs. The progeny viral  
17 particles produced from the tissues subsequently enter the circulation and cause rebound  
18 of plasma viremia, i.e., systemic viral replication.

19           Considering that the state-of-the-art histochemical staining still has lower  
20 sensitivity than PCR and that the vRNA distributions for animals on ART and those  
21 with rebound of plasma viremia are similar, analyses of animals undergoing rebound of  
22 plasma viremia after discontinuation of therapy could serve as a surrogate approach to  
23 study virus reservoirs during HAART.

24           Fortunately, we captured ongoing rebound of plasma viremia in animal  
25 MM511, whose viral burden was above the detection limit defined by the current  
26 staining technique. Further fine-tuning in the duration of therapy and timing of analysis  
27 after cessation would provide better clues to the identity of virus reservoirs.

28

## MATERIALS AND METHODS

### Cells

Human embryonic kidney-derived 293T cells were cultured in Dulbecco's modified Eagle's medium (D-MEM; Invitrogen, Carlsbad, CA) that was supplemented with 10% fetal bovine serum (FBS; HyClone Laboratories, Logan, UT) and 2 mM L-glutamine. Human T-lymphoid MT-4 (Harada et al., 1985), Molt-4 (Koyanagi et al., 1986), and M8166 (Shibata et al., 1991) cells were cultured in RPMI 1640 medium (Invitrogen) that was supplemented with 10% FBS, 2 mM sodium pyruvate, and 4 mM L-glutamine (R-10). Rhesus macaque PBMCs were prepared from whole blood that was anticoagulated with EDTA in lymphocyte separation medium (Nakalai Tesque, Kyoto, Japan). PBMCs were resuspended in R-10 medium that was supplemented with 40 µg/ml gentamicin, 50 µM 2-mercaptoethanol, and 25 µg/ml concanavalin A (Sigma-Aldrich, St. Louis, MO), and cultured for 16–20 h at 37°C. Before virus infection, the cells were cultured for an additional 2 days in R-10 medium that was supplemented with 40 µg/ml gentamicin, 50 µM 2-mercaptoethanol, and 100 IU/ml recombinant human IL-2 (Imunace; Shionogi, Osaka, Japan).

### Viruses

The stock of SIV239 used in the tissue culture and animal experiments was prepared in Rhesus macaque PBMCs inoculated with the supernatant of a 293T-cell culture that was transiently transfected with full-length infectious molecular clones of the virus (Kestler et al., 1990). A stock of HIV-1 IIIB (Popovic et al., 1984) was prepared from the supernatant of a Molt-4 cell culture that was chronically infected with the virus. The SIV239 stock was titrated by infection of M8166 cells, and the number of infectious units was calculated by a method described previously (Reed and Muench, 1938).

### Animal experiments

Female Rhesus macaques of Chinese or Indian origin, 4 kg in body weight, were used for experimental infection with SIV239. Phlebotomy and virus inoculation were carried out under anesthesia by intramuscular injection of a mixture of ketamine chloride (Ketalar; Daiichi Sankyo, Tokyo, Japan) at 5–10 mg/kg and xylazine chloride (Celactal; Bayer Healthcare, Leverkusen, Germany) at 1.5–2.0 mg/kg. For virus

1 infection, animals were inoculated intravenously with 2000-times the 50% tissue culture  
2 infectious doses (TCID<sub>50</sub>) of SIV239. Animal experiments were conducted in a  
3 biosafety level 3 animal facility, in compliance with institutional regulations approved  
4 by the Committee for Experimental Use of Nonhuman Primates of the Institute for  
5 Virus Research, Kyoto University, Kyoto, Japan.

#### 6 7 **Extraction of active components from drug tablets or plasma**

8 Saquinavir (Invirase; Chugai Pharmaceutical, Tokyo, Japan),  
9 Lopinavir/Ritonavir (Kaletra; Abbott Laboratories, Abbott Park, IL), and Atazanavir  
10 (Reyataz; Bristol-Myers Squibb, New York, NY) were purchased from their respective  
11 sources. Drug tablets were pulverized with a pestle and mortar and dissolved in  
12 dimethyl sulfoxide (DMSO; Wako Pure Chemical Industries, Osaka, Japan). The  
13 concentration of each drug in DMSO was adjusted to 100 µg/ml with RPMI 1640  
14 medium. To simulate the conditions of the drugs in the blood, the drug solutions were  
15 diluted 10-fold with normal plasma from Rhesus macaque. The drug extract was  
16 subsequently deproteinized by mixing with methanol/acetonitrile (1:1). The soluble  
17 fraction was evaporated, subsequently reconstituted in RPMI 1640 medium, and  
18 adjusted to a concentration of 20 µg/ml. Plasma samples collected from the animals  
19 were deproteinized, evaporated, and reconstituted as described above. The efficacy of  
20 the extraction employed in the current study ranged from 30-50% when assessed using  
21 the anti-HIV-1 drugs AZT, SQV, and RTV (data not shown).

#### 22 23 **Virus inhibition assay (MT-4/MTT assay)**

24 The efficacies of the PIs against SIV were assessed as described previously  
25 (Sato et al., 1995), with minor modifications. Briefly, aliquots of  $5 \times 10^3$  MT-4 cells were  
26 dispensed into 96-well round-bottomed tissue culture plates. Serially diluted extracts of  
27 the HIV-1 PIs or extracts of animal plasma samples were incubated with the cells in  
28 quadruplicate at 37°C for 1 h. The cells were then inoculated with  $1.8 \times 10^3$  TCID<sub>50</sub> of  
29 SIV239 or  $0.9 \times 10^2$  TCID<sub>50</sub> of HIV-1 IIIB (multiplicity of infection [MOI] = 0.37 or  
30 0.018, respectively). On Day 5 pi, the viability of the cells was assessed by adding the  
31 MTT reagent (Nakalai Tesque).

#### 32 33 **Formulation and feeding of drugs and diet**

1           The daily dosages of the drugs were half of those recommended for an adult  
2 human, i.e., 300 mg of AZT and 150 mg of 3TC (as Combivir; GlaxoSmithKline,  
3 London, UK), 150 mg of Tenofovir disoproxil fumarate (TDF, as Viread; Japan Tobacco,  
4 Tokyo, Japan), and 400 mg of Lopinavir and 100 mg of Ritonavir (as Kaletra; Abbott).  
5 To correlate these dosages for a 4-kg Rhesus macaque with the recommended dosage  
6 for an adult human, the body surface area (BSA) of the monkeys was computed as  
7 described previously (Du Bois and Du Bois, 1915; Du Bois and Du Bois, 1916). Using  
8 BSA and body weight, the *Km* factor for each animal was derived as described  
9 (Reagan-Shaw et al., 2008). The dosage for the monkeys corresponded to 3-fold that for  
10 an adult human weighing 60 kg. Among the drugs selected, Combivir (AZT/3TC) and  
11 Kaletra (LPV/RTV) should be taken twice a day to maintain effective drug  
12 concentrations. Therefore, two sets of drug/diet were prepared. Formulation #1  
13 contained AZT, 3TC, LPV, and RTV (150 mg, 75 mg, 200 mg, and 50 mg, respectively),  
14 while formulation #2 contained all the drugs in formulation #1 plus TDF (150 mg).  
15 Thirty-five grams of primate diet for Old World monkeys (Lab Diet 5048; PMI  
16 Nutrition International, Henderson, CO), granulated with a bar blender, were combined  
17 with the pulverized drugs. The drug/diet mixture was further mixed with 75 g of  
18 squashed banana and formed into a rectangular plate. The formulated drug/diet  
19 described above was given to animals in place of their normal diet. Drug/diet  
20 formulation #1 was given in the morning and formulation #2 was given 10 h later, at  
21 intervals of 10 h and 14 h per day. Seven of the nine Rhesus macaques that were fed the  
22 formulated drug/diet ingested 80-90% of total mass within 2 h.

23           To assess the potential adverse effects of the high-dosage drug  
24 administration employed in the current study, serum samples collected from these  
25 animals before and during cART were submitted to analyses for the following clinical  
26 markers: blood urea nitrogen (BUN), creatinine, total cholesterol, and triglycerides. No  
27 substantial fluctuations were observed before and during cART in the values for BUN  
28 (average values: for MM491, 16.8 mg/dl; for MM499, 16.0 mg/dl; for MM528, 16.7  
29 mg/dl; and for MM530, 20.9 mg/dl), creatinine (average values: for MM491, 0.5 mg/dl;  
30 for MM499, 0.6 mg/dl; for MM528, 0.5 mg/dl; and for MM530, 0.5 mg/dl), and total  
31 cholesterol (average values: for MM491, 153 mg/dl; for MM499, 106 mg/dl; for  
32 MM528, 109 mg/dl; and for MM530, 132 mg/dl). Nearly all the samples analyzed fell  
33 within the normal value ranges for the above-mentioned markers (data not shown). The

1 triglyceride values from all the treated animals, with the exception of MM499,  
2 increased upon onset of ART: for MM491, the values ranged from 28 mg/dl at  
3 pretreatment to 99 mg/dl at maximum during cART; for MM528, from 21 mg/dl to 58  
4 mg/dl; and for MM530, from 48 mg/dl to 129 mg/dl. The published normal value range  
5 for triglycerides in Rhesus macaques is 24–42 mg/dl (Fortman et al., 2001). At autopsy,  
6 lipid deposition in the liver was noted in MM530, which exhibited the highest mean  
7 level of triglycerides among the three animals, indicative of a certain degree of  
8 dysregulation of lipid metabolism. Despite the increase in triglyceride levels, all the  
9 treated animals were clinically healthy.

### 11 **Lopinavir measurement by high-performance liquid chromatography**

12 The drug concentrations in the blood samples were measured by  
13 high-performance liquid chromatography (HPLC) as described previously (Frappier et  
14 al., 1998), with minor modifications. Briefly, plasma samples collected from two  
15 monkeys were subjected to deproteinization by the addition of acetonitrile, and were  
16 subsequently loaded onto a HPLC column. The assay conditions were as follows:  
17 column, ODS column (150 mm in length and 4.6 mm in diameter; Cadenza); mobile  
18 phase, gradient prepared from two solutions (solution A, 0.1% trifluoroacetic acid  
19 [TFA] in water; solution B, 0.1% TFA in acetonitrile). The total flow rate was 0.6  
20 ml/min. For detection of the compound, UV absorbance at a wavelength of 215 nm was  
21 employed.

### 23 **Plasma viral RNA measurement**

24 Viral RNA loads in plasma were measured as described previously (Miyake  
25 et al., 2006). Briefly, total RNA was extracted from plasma samples with the QIAamp  
26 Viral RNA kit (Qiagen, Valencia, CA). The extracted RNA samples were subjected to  
27 RT-PCR to amplify the SIV gag region using the TaqMan EZ RT-PCR kit (PerkinElmer,  
28 Wellesley, MA). The PCR and detection of products were performed in a Prism 7700  
29 Sequence Detector (Applied Biosystems, Foster City, CA). The primer pair employed  
30 for PCR amplification was SIV2-696F  
31 (5'-GGAAATTACCCAGTACAACAAATAFF-3') and SIV2-784R  
32 (5'-TCTATCAATTTTACCCAggCATTTA-3'). PCR products were detected with a  
33 labeled probe, SIV2-731T (5'-Fam-TGTCCACCTGCCATTAAGCCCG-Tamra-3');

1 Perkin Elmer).

2 Selected plasma samples from monkeys on cART (at 29, 42, and 52 weeks pi,  
3 and at euthanasia) were further subjected to quantitative real-time PCR with a lower  
4 detection limit, following the method described by Cline *et al.*, with modifications  
5 (Cline et al., 2005). Briefly, 1.5-ml plasma samples were centrifuged at  $20,000 \times g$  for 1  
6 h to sediment virus particles. The pellets were incubated with a mixture of GuHCl  
7 (Sigma-Aldrich) and proteinase K (Invitrogen) for 60 min at  $37^{\circ}\text{C}$  and subsequently  
8 incubated with a mixture of GuSCN (Sigma-Aldrich) and glycogen (Roche Applied  
9 Science, Indianapolis, IN) for 5 min at room temperature, followed by precipitation with  
10 isopropanol. The precipitated RNA fractions were resuspended in water and subjected  
11 to RT-PCR, as described above. A standard curve of the reaction was constructed by  
12 plotting threshold cycles of serially diluted virus stocks containing known amounts of  
13 vRNA extracted in the same manner as the test plasma samples. The detection limit was  
14 defined by the standard curve with a correlation coefficient ( $> 0.96$ ) constructed from a  
15 set of serial dilutions with reproducible amplification. The detection limit of the assay  
16 was consistently  $< 20$  copies/ml.

17

### 18 **Mathematical modeling and statistical analysis of decay rate**

19 The decline in SIV239 RNA copies in the plasma during cART was evaluated  
20 using a mathematical model similar to that developed previously to quantify and  
21 analyze the decay of HIV-1 viremia in patients treated with combination anti-retroviral  
22 therapy (Perelson et al., 1997). Briefly, two distinct cellular compartments are assumed  
23 to contribute to the vRNA. The first compartment consists of  $\text{CD4}^+$  T cells (i.e.,  
24 short-lived cells),  $T$ , which are infected with a constant,  $k$ , die with a rate constant,  $\delta$ ,  
25 and have a burst size of  $N$ . The second compartment consists of long-lived cells,  $M$ ,  
26 which become infected with a rate constant,  $k_M$ , die with a rate,  $\mu_M$ , and produce  $p$   
27 virions per cell. Free virus particles are cleared with a constant,  $c$ . Assuming that viral  
28 inhibition by cART is  $100\%$ , *de novo* infection is completely blocked in this  
29 mathematical model. Then, using the parameters explained above, the overall vRNA



1 copies in the plasma can be described by the following equation:

$$2 \quad V(t) = V_0 \left\{ \left( 1 - \frac{NkT_0}{c - \delta} - \frac{c - NkT_0}{c - \mu_M} \right) e^{-ct} + \frac{NkT_0}{c - \delta} e^{-\delta t} + \frac{c - NkT_0}{c - \mu_M} e^{-\mu_M t} \right\}. \quad (1)$$

3 Here,  $V_0$  and  $T_0$  are the steady-state level of viral load and CD4<sup>+</sup> T cells  
4 count before HAART, respectively. The derivation of equation (1) is explained in detail  
5 elsewhere (Perelson and Nelson, 1999). To fit the plasma viremia data with the  
6 two-compartment model, we estimated the parameters,  $\delta$ ,  $\mu_M$ , and a composite  
7 parameter,  $NkT_0$ , employing nonlinear least-squares regression (FindMinimum  
8 package of Mathematica ver. 7.0 software). Since virion clearance occurs too rapidly to  
9 estimate  $c$  from the available data in Rhesus macaques, we fixed  $c = 62.1$  (determined  
10 previously) (Igarashi et al., 1999), although the change in  $c$  did not significantly change  
11 in our parameter estimates (data not shown). To derive the 68% confidence interval for  
12 each parameter, we employed a bootstrap method (Efron, 1979; Efron and Tibshirani,  
13 1986) in which each experiment was simulated 1000 times. Statistical comparisons for  
14 continuously distributed variables between groups were performed with Welch's test.  
15 Nominal  $P$ -values  $<0.05$  were considered statistically significant and all tests were  
16 two-sided.

### 17 **Necropsy and tissue collection**

19 All the animals were subjected to perfusion/euthanasia, as described  
20 previously (Igarashi et al., 2002), with minor modifications. Briefly, animals  
21 anesthetized with ketamine/xylazine were intravenously administered pentobarbital  
22 sodium (50 mg/kg body weight, Nembutal; Abbott Laboratories) before thoracotomy.  
23 The right atrium was incised and one liter of sterile saline anti-coagulated with heparin  
24 (5 U/ml) was introduced into the left ventricle *via* a 16G needle attached to infusion  
25 tubing. Peripheral blood was collected prior to perfusion. During the perfusion, tissue  
26 collection was conducted. Collected tissues were trimmed and placed into two  
27 independent workflows: submersion in RNAlater (Qiagen) and stored at -20°C until  
28 RNA extraction, and fixation in 4% paraformaldehyde in PBS at 4°C overnight,  
29 followed by embedding in paraffin wax for histopathologic analyses. The list of

1 collected tissues is summarized in Table 5.

### 3 **Isolation, quantification, and statistical analysis of viral RNA from tissues**

4 Tissues submerged in RNAlater and stored at -20°C were subjected to total  
5 RNA extraction using TRIzol reagent (Invitrogen) according to the manufacturer's  
6 recommendations. Briefly, 50–100 mg of each tissue resuspended in 1 ml of TRIzol  
7 reagent were homogenized with Lysing Matrix D (MP Biomedicals, Irvine, CA) using  
8 FastPrep FP120 (MP Biomedicals). Chloroform (0.2 ml) was added to the homogenate,  
9 and the aqueous phase was collected to a new tube after centrifugation at 12,000 × g for  
10 15 minutes at 4°C. The aqueous phase was mixed with 0.5 ml isopropanol, and the  
11 supernatant was removed after centrifugation at 12,000 × g for 10 minutes at 4°C. Then,  
12 1 ml of 75% ethanol was added to the pellet and, after centrifugation at 7,500 × g for 5  
13 minutes at 4°C, the supernatant was cleared. The total RNA sample was resuspended in  
14 RNase-free water and frozen at -80°C until use. The amount of RNA extracted from  
15 each tissue specimen was measured in a UV spectrophotometer (UV-1600; Shimadzu,  
16 Kyoto, Japan). Aliquots (1 µg) of RNA extracted from the various tissue samples were  
17 subjected to RT-PCR, to amplify the SIV gag region. The amounts of vRNA detected by  
18 PCR in a variety of tissues from treated animals and untreated controls, as described  
19 below, were compared using a Mann-Whitney test and GraphPad Prism software  
20 (GraphPad, La Jolla, CA).

### 22 **Immunohistochemistry**

23 Viral-protein-producing cells were visualized with an anti-SIV antibody and  
24 anti-CD35 antibody, as described previously (Inaba et al., 2009), with minor  
25 modifications. Briefly, tissue sections (4-µm thickness) were dewaxed with xylene,  
26 rehydrated through an alcohol gradient, submerged in Target Retrieval Solution (DAKO,  
27 Glostrup, Denmark), and processed in an autoclave for 10 min to unmask the antigens.  
28 Subsequently, the tissue sections were washed with Tris-buffered saline/Tween-20  
29 (TBST), treated with REAL Peroxidase-Blocking Solution (DAKO) for 5 min, to  
30 deactivate endogenous peroxidase, and washed with TBST. The sections were incubated  
31 with an anti-SIV Nef mouse monoclonal antibody (diluted 1:500, clone 04-001; FIT  
32 Biotech, Tampere, Finland) at 4°C overnight. After washing with TBST, the sections  
33 were incubated at room temperature for 30 min with the Envision+ kit (a horseradish

1 peroxidase-labeled anti-mouse immunoglobulin polymer; DAKO), washed with TBST,  
2 visualized using diaminobenzidine (DAB) substrate (DAKO) as the chromogen, and  
3 rinsed in distilled water. Subsequently, the sections were treated at 95°C for 10 min with  
4 Target Retrieval Solution (DAKO), to deactivate the antibody added upstream in the  
5 procedure, washed with TBST, and incubated with the anti-CD35 mouse monoclonal  
6 antibody (diluted 1:50, clone Ber-MAC-DRC; DAKO) at 4°C overnight. After washing,  
7 the slides were incubated with Histofine Simple Stain AP (an alkaline  
8 phosphatase-labeled anti-mouse immunoglobulin polymer; Nichirei, Tokyo, Japan) at  
9 room temperature for 30 min, and washed with TBST. The specific antigen-antibody  
10 reaction was visualized with Blue Alkaline Phosphatase Substrate Kit III (Vector  
11 Laboratories, Burlingame, CA). The stained sections were examined under an Axiophot  
12 Universal microscope (Carl Zeiss, Oberkochen, Germany), and images were captured  
13 with the Nikon Digital Sight DS-Fi1 camera head and Nikon Digital Sight DS-L2  
14 control unit (Nikon, Tokyo, Japan).

15 To identify the Nef-producing cells, slides of the tissue were stained with the  
16 anti-SIV antibody and anti-CD3 antibody. Sections were subjected to dewaxing and  
17 unmasking of antigens, as described above. Subsequently, the sections were incubated  
18 with the anti-SIV Nef mouse monoclonal antibody (diluted 1:500, clone 04-001; FIT  
19 Biotech) at 4°C overnight. After washing with TBST, the sections were incubated at  
20 room temperature for 30 min with anti-CD3 rabbit polyclonal antibody (diluted 1:50;  
21 DAKO), and washed with TBST. The sections were treated with Alexa Fluor 488  
22 (diluted 1:200, fluorochrome-conjugated goat anti-mouse immunoglobulin G;  
23 Molecular Probes, Eugene, OR) and Alexa Fluor 594 (diluted 1:200;  
24 fluorochrome-conjugated goat anti-rabbit immunoglobulin G; Molecular Probes) for 1  
25 hour, to visualize the bound anti-SIV Nef antibody and anti-CD3 antibody, respectively.  
26 The stained sections were examined using a Leica TCS SP2 AOBS confocal microscope  
27 (Leica Microsystems, Exton, PA) and the Leica image software (Leica Microsystems).  
28 Sections prepared from an SIV-infected monkey (MM521) and uninfected monkeys  
29 were stained in the same manner as those from cART and post-cART animals, as  
30 controls for the staining (Supplemental Figure 3).

31

1

2

## ACKNOWLEDGEMENT

3

4

5

6

7

8

9

10

11

## REFERENCES

12

13

14

15

16

17

18

19

20

21

22

23

24

25

26

27

28

29

30

The authors are in debt to Drs. T. Sata and S. Nakamura for technical advice and critique on histochemical staining, Dr. A. Nomoto for continuous support, and member of the Igarashi laboratory for assistance of animal procedures and analyses. This work was supported by Research on HIV/AIDS [08062160 to T.I.] from the Ministry of Health, Labor and Welfare of Japan. S.I. was supported by JST PRESTO program.

Balzarini, J., Weeger, M., Camarasa, M. J., De Clercq, E., and Uberla, K., 1995. Sensitivity/resistance profile of a simian immunodeficiency virus containing the reverse transcriptase gene of human immunodeficiency virus type 1 (HIV-1) toward the HIV-1-specific non-nucleoside reverse transcriptase inhibitors. *Biochem Biophys Res Commun.* 211 (3), 850-6.

Benlhassan-Chahour, K., Penit, C., Dioszeghy, V., Vasseur, F., Janvier, G., Riviere, Y., Dereuddre-Bosquet, N., Dormont, D., Le Grand, R., and Vaslin, B., 2003. Kinetics of lymphocyte proliferation during primary immune response in macaques infected with pathogenic simian immunodeficiency virus SIVmac251: preliminary report of the effect of early antiviral therapy. *J Virol.* 77 (23), 12479-93.

Bourry, O., Mannioui, A., Sellier, P., Roucairol, C., Durand-Gasselien, L., Dereuddre-Bosquet, N., Benech, H., Roques, P., and Le Grand, R., 2010. Effect of a short-term HAART on SIV load in macaque tissues is dependent on time of initiation and antiviral diffusion. *Retrovirology.* 7, 78.

Brenchley, J. M., Schacker, T. W., Ruff, L. E., Price, D. A., Taylor, J. H.,

- 1 Beilman, G. J., Nguyen, P. L., Khoruts, A., Larson, M., Haase, A. T.,  
2 and Douek, D. C., 2004. CD4+ T cell depletion during all stages of HIV  
3 disease occurs predominantly in the gastrointestinal tract. *J Exp Med.*  
4 200 (6), 749-59.
- 5 Brennan, T. P., Woods, J. O., Sedaghat, A. R., Siliciano, J. D., Siliciano, R. F.,  
6 and Wilke, C. O., 2009. Analysis of human immunodeficiency virus  
7 type 1 viremia and provirus in resting CD4+ T cells reveals a novel  
8 source of residual viremia in patients on antiretroviral therapy. *J Virol.*  
9 83 (17), 8470-81.
- 10 Burton, G. F., Keele, B. F., Estes, J. D., Thacker, T. C., and Gartner, S., 2002.  
11 Follicular dendritic cell contributions to HIV pathogenesis. *Semin*  
12 *Immunol.* 14 (4), 275-84.
- 13 Buzon, M. J., Massanella, M., Llibre, J. M., Esteve, A., Dahl, V., Puertas, M.  
14 C., Gatell, J. M., Domingo, P., Paredes, R., Sharkey, M., Palmer, S.,  
15 Stevenson, M., Clotet, B., Blanco, J., and Martinez-Picado, J., 2010.  
16 HIV-1 replication and immune dynamics are affected by raltegravir  
17 intensification of HAART-suppressed subjects. *Nat Med.* 16 (4), 460-5.
- 18 Chun, T. W., Davey, R. T., Jr., Engel, D., Lane, H. C., and Fauci, A. S., 1999.  
19 Re-emergence of HIV after stopping therapy. *Nature.* 401 (6756),  
20 874-5.
- 21 Chun, T. W., Davey, R. T., Jr., Ostrowski, M., Shawn Justement, J., Engel, D.,  
22 Mullins, J. I., and Fauci, A. S., 2000. Relationship between  
23 pre-existing viral reservoirs and the re-emergence of plasma viremia  
24 after discontinuation of highly active anti-retroviral therapy. *Nat Med.*  
25 6 (7), 757-61.
- 26 Chun, T. W., Stuyver, L., Mizell, S. B., Ehler, L. A., Mican, J. A., Baseler, M.,  
27 Lloyd, A. L., Nowak, M. A., and Fauci, A. S., 1997. Presence of an  
28 inducible HIV-1 latent reservoir during highly active antiretroviral  
29 therapy. *Proc Natl Acad Sci U S A.* 94 (24), 13193-7.
- 30 Cline, A. N., Bess, J. W., Piatak, M., Jr., and Lifson, J. D., 2005. Highly  
31 sensitive SIV plasma viral load assay: practical considerations,  
32 realistic performance expectations, and application to reverse  
33 engineering of vaccines for AIDS. *J Med Primatol.* 34 (5-6), 303-12.

- 1 Connick, E., Mattila, T., Folkvord, J. M., Schlichtemeier, R., Meditz, A. L.,  
2 Ray, M. G., McCarter, M. D., Mawhinney, S., Hage, A., White, C., and  
3 Skinner, P. J., 2007. CTL fail to accumulate at sites of HIV-1  
4 replication in lymphoid tissue. *J Immunol.* 178 (11), 6975-83.
- 5 Dinoso, J. B., Rabi, S. A., Blankson, J. N., Gama, L., Mankowski, J. L.,  
6 Siliciano, R. F., Zink, M. C., and Clements, J. E., 2009. A simian  
7 immunodeficiency virus-infected macaque model to study viral  
8 reservoirs that persist during highly active antiretroviral therapy. *J*  
9 *Virol.* 83 (18), 9247-57.
- 10 Douek, D. C., Picker, L. J., and Koup, R. A., 2003. T cell dynamics in HIV-1  
11 infection. *Annu Rev Immunol.* 21, 265-304.
- 12 Du Bois, D., and Du Bois, E. F., 1915. The measurement of the surface area  
13 of man. *Archives of Internal Medicine.* 15, 868-881.
- 14 Du Bois, D., and Du Bois, E. F., 1916. A formula to estimate the approximate  
15 surface area if height and weight be known. *Archives of Internal*  
16 *Medicine.* 17, 863-871.
- 17 Efron, B., 1979. 1977 Rietz Lecture - Bootstrap Methods - Another Look at  
18 the Jackknife. *Annals of Statistics.* 7 (1), 1-26.
- 19 Efron, B., and Tibshirani, R., 1986. Bootstrap methods for standard errors,  
20 confidence intervals, and other measures of statistical accuracy.  
21 *Statistical Science* 1,54-75.
- 22 Embretson, J., Zupancic, M., Ribas, J. L., Burke, A., Racz, P., Tenner-Racz,  
23 K., and Haase, A. T., 1993. Massive covert infection of helper T  
24 lymphocytes and macrophages by HIV during the incubation period of  
25 AIDS. *Nature.* 362 (6418), 359-62.
- 26 Finzi, D., Hermankova, M., Pierson, T., Carruth, L. M., Buck, C., Chaisson, R.  
27 E., Quinn, T. C., Chadwick, K., Margolick, J., Brookmeyer, R., Gallant,  
28 J., Markowitz, M., Ho, D. D., Richman, D. D., and Siliciano, R. F., 1997.  
29 Identification of a reservoir for HIV-1 in patients on highly active  
30 antiretroviral therapy. *Science.* 278 (5341), 1295-300.
- 31 Folkvord, J. M., Armon, C., and Connick, E., 2005. Lymphoid follicles are  
32 sites of heightened human immunodeficiency virus type 1 (HIV-1)  
33 replication and reduced antiretroviral effector mechanisms. *AIDS Res*

- 1 Hum Retroviruses. 21 (5), 363-70.
- 2 Fortman, J. D., Hewett, T. A., and Bennett, B. T., 2001. The Laboratory  
3 Nonhuman Primate. CRC Press, New York.
- 4 Frappier, S., Breilh, D., Diarte, E., Ba, B., Ducint, D., Pellegrin, J. L., and  
5 Saux, M. C., 1998. Simultaneous determination of ritonavir and  
6 saquinavir, two human immunodeficiency virus protease inhibitors, in  
7 human serum by high-performance liquid chromatography. J  
8 Chromatogr B Biomed Sci Appl. 714 (2), 384-9.
- 9 Frost, S. D., Gunthard, H. F., Wong, J. K., Havlir, D., Richman, D. D., and  
10 Leigh Brown, A. J., 2001. Evidence for positive selection driving the  
11 evolution of HIV-1 env under potent antiviral therapy. Virology. 284  
12 (2), 250-8.
- 13 Giuffre, A. C., Higgins, J., Buckheit, R. W., Jr., and North, T. W., 2003.  
14 Susceptibilities of simian immunodeficiency virus to protease  
15 inhibitors. Antimicrob Agents Chemother. 47 (5), 1756-9.
- 16 Guadalupe, M., Reay, E., Sankaran, S., Prindiville, T., Flamm, J., McNeil, A.,  
17 and Dandekar, S., 2003. Severe CD4+ T-cell depletion in gut lymphoid  
18 tissue during primary human immunodeficiency virus type 1 infection  
19 and substantial delay in restoration following highly active  
20 antiretroviral therapy. J Virol. 77 (21), 11708-17.
- 21 Harada, S., Koyanagi, Y., and Yamamoto, N., 1985. Infection of  
22 HTLV-III/LAV in HTLV-I-carrying cells MT-2 and MT-4 and  
23 application in a plaque assay. Science. 229 (4713), 563-6.
- 24 Havlir, D. V., Strain, M. C., Clerici, M., Ignacio, C., Trabattoni, D., Ferrante,  
25 P., and Wong, J. K., 2003. Productive infection maintains a dynamic  
26 steady state of residual viremia in human immunodeficiency virus  
27 type 1-infected persons treated with suppressive antiretroviral  
28 therapy for five years. J Virol. 77 (20), 11212-9.
- 29 Igarashi, T., Brown, C., Azadegan, A., Haigwood, N., Dimitrov, D., Martin, M.  
30 A., and Shibata, R., 1999. Human immunodeficiency virus type 1  
31 neutralizing antibodies accelerate clearance of cell-free virions from  
32 blood plasma. Nat Med. 5 (2), 211-6.
- 33 Igarashi, T., Brown, C. R., Byrum, R. A., Nishimura, Y., Endo, Y., Plishka, R.

1 J., Buckler, C., Buckler-White, A., Miller, G., Hirsch, V. M., and Martin,  
2 M. A., 2002. Rapid and irreversible CD4+ T-cell depletion induced by  
3 the highly pathogenic simian/human immunodeficiency virus  
4 SHIV(DH12R) is systemic and synchronous. *J Virol.* 76 (1), 379-91.

5 Inaba, K., Fukazawa, Y., Matsuda, K., Himeno, A., Matsuyama, M., Ibuki, K.,  
6 Miura, Y., Koyanagi, Y., Nakajima, A., Blumberg, R. S., Takahashi, H.,  
7 Hayami, M., Igarashi, T., and Miura, T., 2009. Small intestine CD4+  
8 cell reduction and enteropathy in simian/human immunodeficiency  
9 virus KS661-infected rhesus macaques in the presence of low viral  
10 load. *J Gen Virol.* 91 (Pt 3), 773-81.

11 Keele, B. F., Tazi, L., Gartner, S., Liu, Y., Burgon, T. B., Estes, J. D., Thacker,  
12 T. C., Crandall, K. A., McArthur, J. C., and Burton, G. F., 2008.  
13 Characterization of the follicular dendritic cell reservoir of human  
14 immunodeficiency virus type 1. *J Virol.* 82 (11), 5548-61.

15 Kestler, H., Kodama, T., Ringler, D., Marthas, M., Pedersen, N., Lackner, A.,  
16 Regier, D., Sehgal, P., Daniel, M., King, N., and et al., 1990. Induction  
17 of AIDS in rhesus monkeys by molecularly cloned simian  
18 immunodeficiency virus. *Science.* 248 (4959), 1109-12.

19 Koyanagi, Y., Harada, S., and Yamamoto, N., 1986. Establishment of a high  
20 production system for AIDS retroviruses with a human T-leukemic  
21 cell line Molt-4. *Cancer Lett.* 30 (3), 299-310.

22 Markowitz, M., Louie, M., Hurley, A., Sun, E., Di Mascio, M., Perelson, A. S.,  
23 and Ho, D. D., 2003. A novel antiviral intervention results in more  
24 accurate assessment of human immunodeficiency virus type 1  
25 replication dynamics and T-cell decay in vivo. *J Virol.* 77 (8), 5037-8.

26 Martinez, M. A., Cabana, M., Ibanez, A., Clotet, B., Arno, A., and Ruiz, L.,  
27 1999. Human immunodeficiency virus type 1 genetic evolution in  
28 patients with prolonged suppression of plasma viremia. *Virology.* 256  
29 (2), 180-7.

30 Meng, G., Sellers, M. T., Mosteller-Barnum, M., Rogers, T. S., Shaw, G. M.,  
31 and Smith, P. D., 2000. Lamina propria lymphocytes, not macrophages,  
32 express CCR5 and CXCR4 and are the likely target cell for human  
33 immunodeficiency virus type 1 in the intestinal mucosa. *J Infect Dis.*



1 182 (3), 785-91.

2 Miyake, A., Ibuki, K., Enose, Y., Suzuki, H., Horiuchi, R., Motohara, M.,  
3 Saito, N., Nakasone, T., Honda, M., Watanabe, T., Miura, T., and  
4 Hayami, M., 2006. Rapid dissemination of a pathogenic simian/human  
5 immunodeficiency virus to systemic organs and active replication in  
6 lymphoid tissues following intrarectal infection. *J Gen Virol.* 87 (Pt 5),  
7 1311-20.

8 Murray, J. M., Emery, S., Kelleher, A. D., Law, M., Chen, J., Hazuda, D. J.,  
9 Nguyen, B. Y., Teppler, H., and Cooper, D. A., 2007. Antiretroviral  
10 therapy with the integrase inhibitor raltegravir alters decay kinetics  
11 of HIV, significantly reducing the second phase. *AIDS.* 21 (17),  
12 2315-21.

13 North, T. W., Higgins, J., Deere, J. D., Hayes, T. L., Villalobos, A., Adamson,  
14 L., Shacklett, B. L., Schinazi, R. F., and Luciw, P. A., 2009. Viral  
15 sanctuaries during highly active antiretroviral therapy in a  
16 nonhuman primate model for AIDS. *J Virol.* 84 (6), 2913-22.

17 Palmer, S., Maldarelli, F., Wiegand, A., Bernstein, B., Hanna, G. J., Brun, S.  
18 C., Kempf, D. J., Mellors, J. W., Coffin, J. M., and King, M. S., 2008.  
19 Low-level viremia persists for at least 7 years in patients on  
20 suppressive antiretroviral therapy. *Proc Natl Acad Sci U S A.* 105 (10),  
21 3879-84.

22 Pantaleo, G., Graziosi, C., Demarest, J. F., Butini, L., Montroni, M., Fox, C.  
23 H., Orenstein, J. M., Kotler, D. P., and Fauci, A. S., 1993. HIV infection  
24 is active and progressive in lymphoid tissue during the clinically  
25 latent stage of disease. *Nature.* 362 (6418), 355-8.

26 Pauwels, R., Balzarini, J., Baba, M., Snoeck, R., Schols, D., Herdewijn, P.,  
27 Desmyter, J., and De Clercq, E., 1988. Rapid and automated  
28 tetrazolium-based colorimetric assay for the detection of anti-HIV  
29 compounds. *J Virol Methods.* 20 (4), 309-21.

30 Perelson, A. S., Essunger, P., Cao, Y., Vesanen, M., Hurley, A., Saksela, K.,  
31 Markowitz, M., and Ho, D. D., 1997. Decay characteristics of  
32 HIV-1-infected compartments during combination therapy. *Nature.*  
33 387 (6629), 188-91.

1 Perelson, A. S., and Nelson, P. W., 1999. Mathematical analysis of HIV-1  
2 dynamics in vivo. *Siam Review*. 41 (1), 3-44.

3 Popovic, M., Sarngadharan, M. G., Read, E., and Gallo, R. C., 1984.  
4 Detection, isolation, and continuous production of cytopathic  
5 retroviruses (HTLV-III) from patients with AIDS and pre-AIDS.  
6 *Science*. 224 (4648), 497-500.

7 Reagan-Shaw, S., Nihal, M., and Ahmad, N., 2008. Dose translation from  
8 animal to human studies revisited. *FASEB J*. 22 (3), 659-61.

9 Reed, L., and Muench, H., 1938. A simple method of estimating fifty percent  
10 endpoints. *The american journal of hygiene*. 27, 493-497.

11 Richman, D. D., 2001. HIV chemotherapy. *Nature*. 410 (6831), 995-1001.

12 Sato, A., Kodama, M., Abe, K., Miki, S., Nishimura, M., Suyama, A., Ogata,  
13 M., Toyoda, T., Sugimoto, H., Yoshie, O., and et al., 1995. A simple and  
14 rapid method for preliminary evaluation of in vivo efficacy of anti-HIV  
15 compounds in mice. *Antiviral Res*. 27 (1-2), 151-63.

16 Sharkey, M., Babic, D. Z., Greenough, T., Gulick, R., Kuritzkes, D. R., and  
17 Stevenson, M., 2011. Episomal viral cDNAs identify a reservoir that  
18 fuels viral rebound after treatment interruption and that contributes  
19 to treatment failure. *PLoS Pathog*. 7 (2), e1001303.

20 Sharkey, M., Triques, K., Kuritzkes, D. R., and Stevenson, M., 2005. In vivo  
21 evidence for instability of episomal human immunodeficiency virus  
22 type 1 cDNA. *J Virol*. 79 (8), 5203-10.

23 Sharkey, M. E., Teo, I., Greenough, T., Sharova, N., Luzuriaga, K., Sullivan,  
24 J. L., Bucy, R. P., Kostrikis, L. G., Haase, A., Veryard, C., Davaro, R. E.,  
25 Cheeseman, S. H., Daly, J. S., Bova, C., Ellison, R. T., 3rd, Mady, B.,  
26 Lai, K. K., Moyle, G., Nelson, M., Gazzard, B., Shaunak, S., and  
27 Stevenson, M., 2000. Persistence of episomal HIV-1 infection  
28 intermediates in patients on highly active anti-retroviral therapy. *Nat*  
29 *Med*. 6 (1), 76-81.

30 Shibata, R., Kawamura, M., Sakai, H., Hayami, M., Ishimoto, A., and Adachi,  
31 A., 1991. Generation of a chimeric human and simian  
32 immunodeficiency virus infectious to monkey peripheral blood  
33 mononuclear cells. *J Virol*. 65 (7), 3514-20.

- 1 Siliciano, J. D., Kajdas, J., Finzi, D., Quinn, T. C., Chadwick, K., Margolick, J.  
2 B., Kovacs, C., Gange, S. J., and Siliciano, R. F., 2003. Long-term  
3 follow-up studies confirm the stability of the latent reservoir for HIV-1  
4 in resting CD4+ T cells. *Nat Med.* 9 (6), 727-8.
- 5 Spiegel, H., Herbst, H., Niedobitek, G., Foss, H. D., and Stein, H., 1992.  
6 Follicular dendritic cells are a major reservoir for human  
7 immunodeficiency virus type 1 in lymphoid tissues facilitating  
8 infection of CD4+ T-helper cells. *Am J Pathol.* 140 (1), 15-22.
- 9 Thacker, T. C., Zhou, X., Estes, J. D., Jiang, Y., Keele, B. F., Elton, T. S., and  
10 Burton, G. F., 2009. Follicular dendritic cells and human  
11 immunodeficiency virus type 1 transcription in CD4+ T cells. *J Virol.*  
12 83 (1), 150-8.
- 13 Van Rompay, K. K., Brignolo, L. L., Meyer, D. J., Jerome, C., Tarara, R.,  
14 Spinner, A., Hamilton, M., Hirst, L. L., Bennett, D. R., Canfield, D. R.,  
15 Dearman, T. G., Von Morgenland, W., Allen, P. C., Valverde, C.,  
16 Castillo, A. B., Martin, R. B., Samii, V. F., Bendele, R., Desjardins, J.,  
17 Marthas, M. L., Pedersen, N. C., and Bischofberger, N., 2004.  
18 Biological effects of short-term or prolonged administration of  
19 9-[2-(phosphonomethoxy)propyl]adenine (tenofovir) to newborn and  
20 infant rhesus macaques. *Antimicrob Agents Chemother.* 48 (5),  
21 1469-87.
- 22 Veazey, R. S., DeMaria, M., Chalifoux, L. V., Shvetz, D. E., Pauley, D. R.,  
23 Knight, H. L., Rosenzweig, M., Johnson, R. P., Desrosiers, R. C., and  
24 Lackner, A. A., 1998. Gastrointestinal tract as a major site of CD4+ T  
25 cell depletion and viral replication in SIV infection. *Science.* 280  
26 (5362), 427-31.
- 27 Veazey, R. S., Mansfield, K. G., Tham, I. C., Carville, A. C., Shvetz, D. E.,  
28 Forand, A. E., and Lackner, A. A., 2000. Dynamics of CCR5 expression  
29 by CD4(+) T cells in lymphoid tissues during simian  
30 immunodeficiency virus infection. *J Virol.* 74 (23), 11001-7.
- 31 Witvrouw, M., Pannecouque, C., Switzer, W. M., Folks, T. M., De Clercq, E.,  
32 and Heneine, W., 2004. Susceptibility of HIV-2, SIV and SHIV to  
33 various anti-HIV-1 compounds: implications for treatment and

1 postexposure prophylaxis. *Antivir Ther.* 9 (1), 57-65.  
2 Wong, J. K., Hezareh, M., Gunthard, H. F., Havlir, D. V., Ignacio, C. C., Spina,  
3 C. A., and Richman, D. D., 1997. Recovery of replication-competent  
4 HIV despite prolonged suppression of plasma viremia. *Science*. 278  
5 (5341), 1291-5.

6

7

#### WEB REFERENCE

8

9 Department of Health and Human Services (DHHS) (2011). Guidelines for  
10 the use of antiretroviral agents in HIV-1-infected adults and adolescents.  
11 (<http://aidsinfo.nih.gov/contentfiles/AdultandAdolescentGL.pdf>)

12

13

#### FIGURE CAPTIONS

14 **Figure 1.** Effects of cART on plasma viral loads. Seven Rhesus macaques were  
15 inoculated with SIV239. Four animals, MM491, MM499, MM528, and MM530 (solid  
16 lines), were treated with cART (shaded areas). Animals MM510, MM496, and MM521  
17 (dotted line) served as untreated controls. The detection limit of our RT-PCR assay is  
18 200 RNA copies/ml, and samples with levels below the level of detection are plotted as  
19 200 RNA copies/ml. †, time of euthanasia.

20 **Figure 2.** Nef-expressing cells detected in the iMLNs of animal MM511. (a) The  
21 section was stained with the anti-SIV Nef mouse monoclonal antibody. (b)  
22 Juxtaposition of Nef-expressing cells and CD35-positive FDCs in the follicle of an

1 iMLN from MM511. The sample was stained using the anti-SIV Nef mouse monoclonal  
2 antibody (brown) and the anti-CD35 mouse monoclonal antibody (blue). Original  
3 magnification,  $\times 40$ . The insets contain a higher-magnification,  $\times 126$  equivalent  
4 (original magnification,  $\times 63$ ).

5 **Figure 3.** Nef-positive T lymphocytes in the MLN of animal MM511. Tissue sections  
6 were stained using the anti-SIV Nef mouse monoclonal antibody (green, a and d) and  
7 the anti-CD3 rabbit polyclonal antibody (red, b and e). (c) Superimposed image of a and  
8 b. Nef-positive T cells are clustered in the follicles of the iMLN. (f) Superimposed  
9 image of d and e. The T cell is detected in the paracortical area of the sMLN. Original  
10 magnification,  $\times 40$ .

11 **Supplemental Figure 1.** Efficacies of commercially available anti-HIV-1 protease  
12 inhibitors against SIV239 and HIV-1 IIIB. The anti-SIV efficacies of Saquinavir (SQV),  
13 Lopinavir/Ritonavir (LPV/RTV), and Atazanavir (ATV) were evaluated in the  
14 MT-4/MTT assay. HIV-1 IIIB was used as a control virus. Each virus was inoculated to  
15 MT-4 cells in the presence of increasing amounts of extracts from the drug tablets in  
16 quadruplicate. Cell proliferation was assessed with the MTT reagent on Day 5 of  
17 infection.

18 **Supplemental Figure 2.** Decay of plasma viremia in four monkeys in group A that

1 received cART. Plasma viral loads were measured by quantitative RT-PCR. The  
2 theoretical decay curve (dashed bold line) was derived by nonlinear least-square fitting  
3 of the mathematical model of Equation 1 (described in *Materials and Methods*) to the  
4 plasma viral load. The dotted line represents the declination of virus particles produced  
5 by short-lived infected cells,  $V_0 \frac{NkT_0}{c-\delta} e^{-\delta t}$ , and the dot-dashed line expresses the decay of  
6 virions produced by long-lived infected cells,  $V_0 \frac{c-NkT_0}{c-\mu_M} e^{-\mu_M t}$ . The steady-state values of  
7 viral load,  $V_0$ , are averages of measurements obtained at three time-points over 3 weeks  
8 prior to the onset of cART. The parameters  $\delta$ ,  $\mu_M$ , and  $NkT_0$ , were estimated  
9 simultaneously. The parameter estimates are as follows: MM491,  $\delta = 0.495$ ,  
10  $\mu_M = 0.028$ , and  $NkT_0 = 61.90$ ; MM499,  $\delta = 0.853$ ,  $\mu_M = 0.089$ , and  $NkT_0 = 61.44$ ;  
11 MM528,  $\delta = 0.707$ ,  $\mu_M = 0.980$ , and  $NkT_0 = 61.68$ ; MM530,  $\delta = 0.523$ ,  $\mu_M = 0.053$ ,  
12 and  $NkT_0 = 61.78$ .

13 **Supplemental Figure 3.** Sections from the MLNs of untreated animal MM521 (a, b and  
14 c), and an uninfected animal (d, e and f), as positive and negative controls, respectively.  
15 The tissue sections were stained with the anti-SIV Nef mouse monoclonal antibody  
16 (green, a and d) and the anti-CD3 rabbit polyclonal antibody (red, b and e). (c)  
17 Superimposed image of a and b. Nef-positive T cells are observed in the follicles and  
18 the paracortical area of the MLN. (f) Superimposed image of d and e. T cells were not  
19 detected in the sMLN. Original magnification,  $\times 40$ .

Figure1  
[Click here to download high resolution image](#)

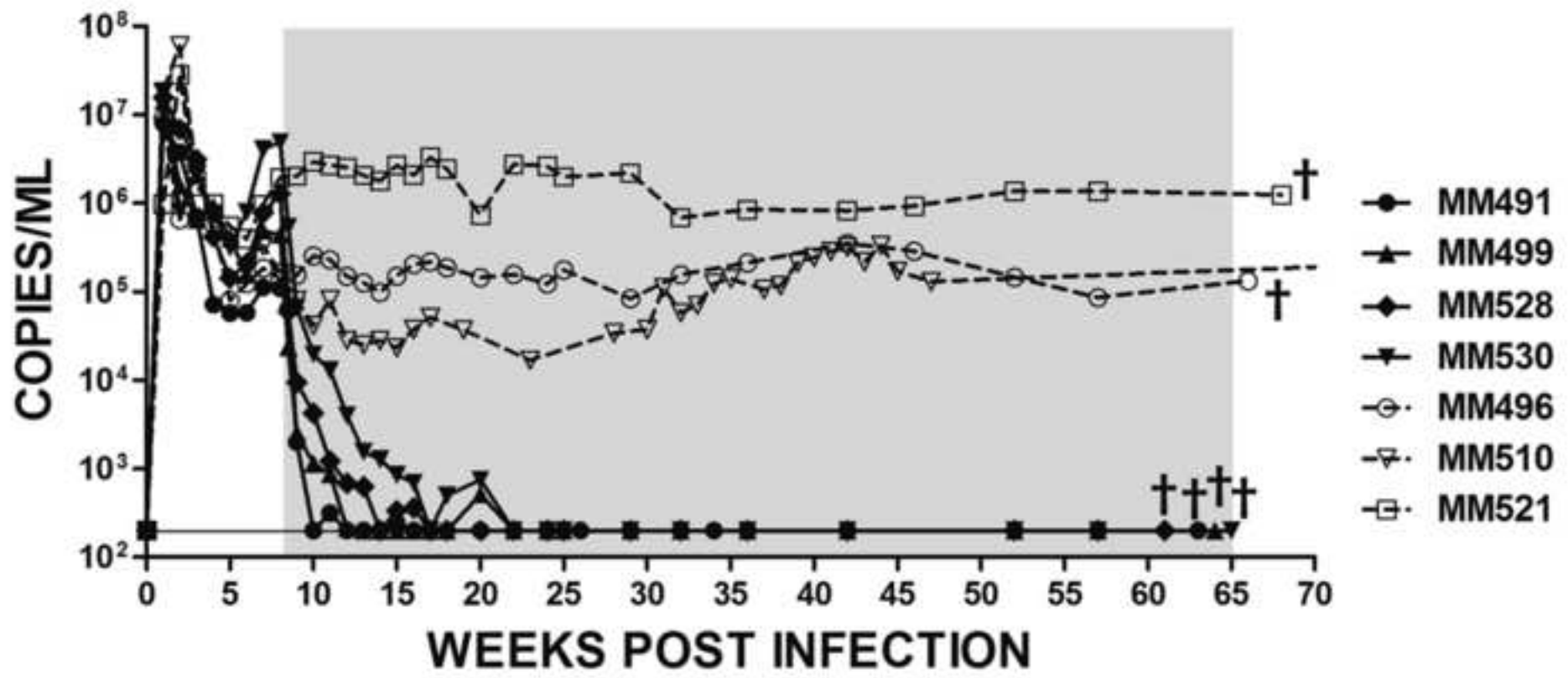


Figure2  
[Click here to download high resolution image](#)

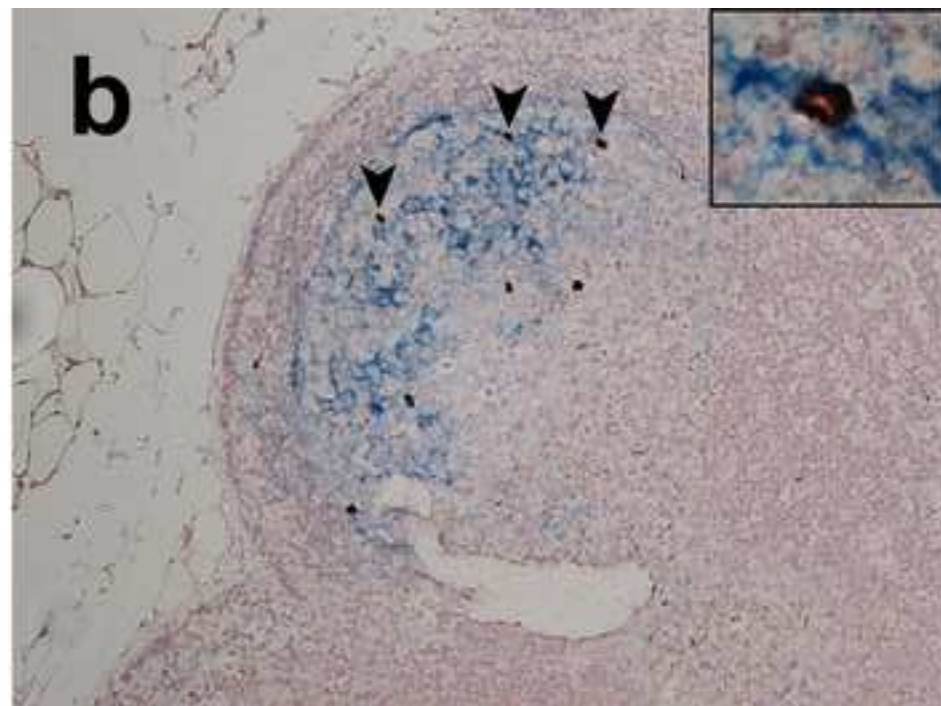
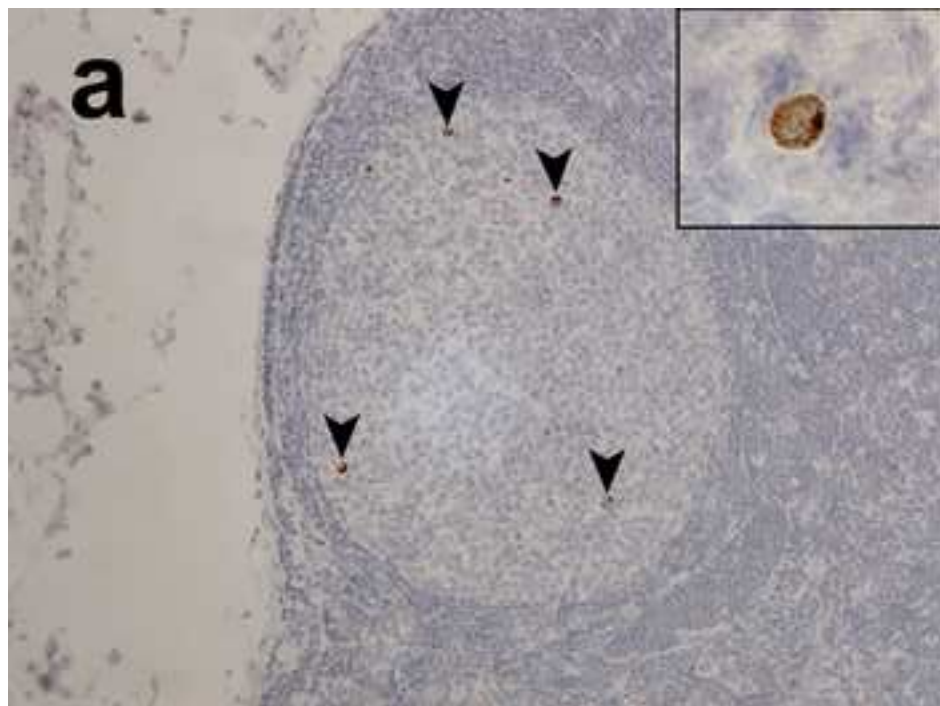
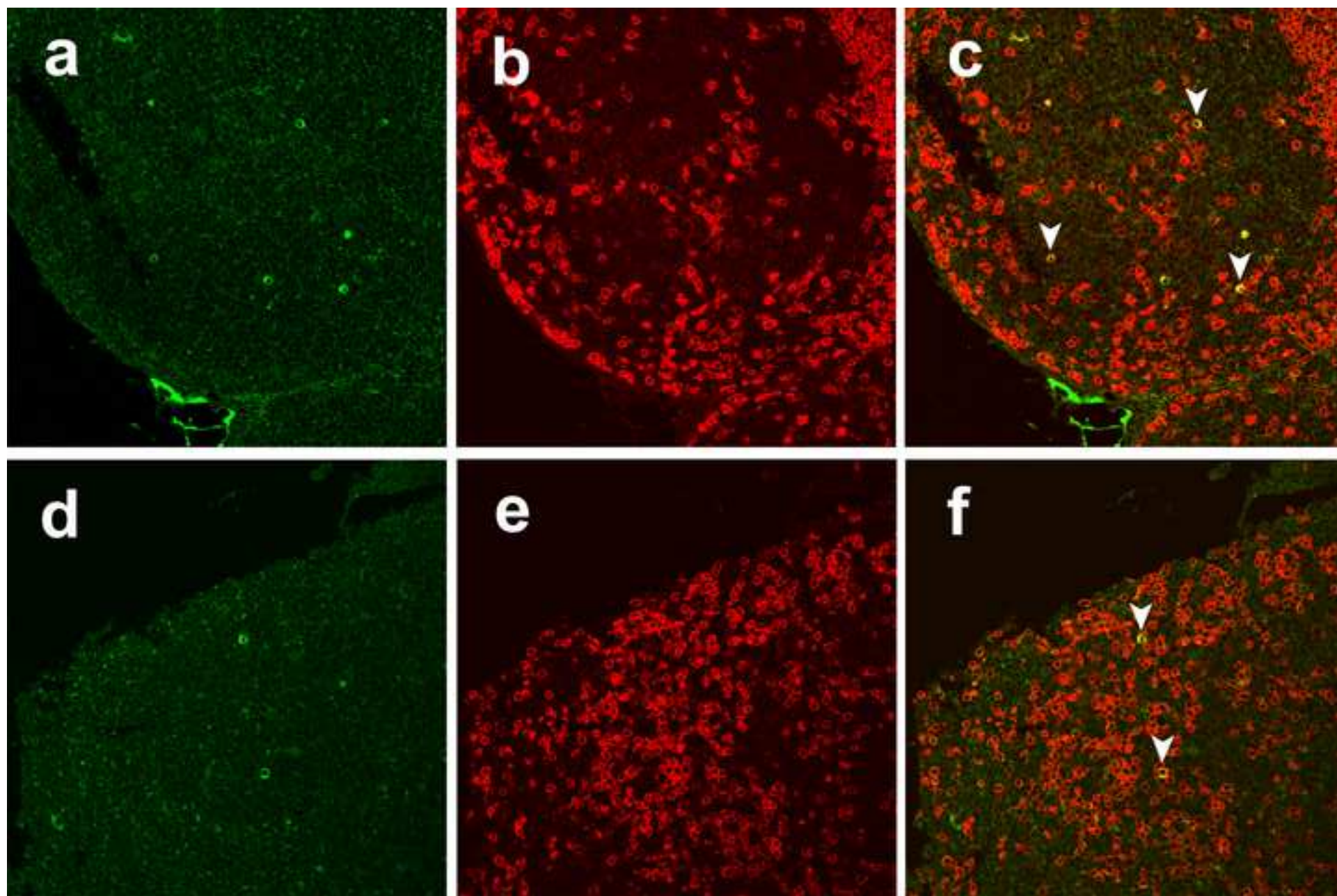




Figure3  
[Click here to download high resolution image](#)



**Table 1.** Efficacies of commercially available anti-HIV-1 protease inhibitors against SIV239 and HIV-1 IIB.

Compounds	EC <sub>50</sub> <sup>a</sup> (nM)		EC <sub>50</sub> ratio <sup>b</sup>
	SIV239	HIV-1 IIB	
Saquinavir	18.5	22.7	0.8
Lopinavir/Ritonavir	52.2	35.6	1.5
Atazanavir	80.0	16.9	4.7

<sup>a</sup>50 % effective concentration

<sup>b</sup>EC<sub>50</sub> value against SIV239 divided by the EC<sub>50</sub> value against HIV-1 IIB.

**Table 2****Table 2.** Decay rate and half-life derived by mathematical modeling of short- or long-lived infected cells in group A monkeys.

Animal ID	Short-lived infected cells		Long-lived infected cells	
	Decay rate : $a$ ( $\text{day}^{-1}$ )	Half-life : $\log_2/a$ (days)	Decay rate : $\mu_M$ ( $\text{day}^{-1}$ )	Half-life : $\log_2/\mu_M$ (days)
MM491	0.495 [0.405-0.605] <sup>a</sup>	1.400 [1.146-1.711]	0.028 [0.000-0.141]	24.76 [4.916- $\infty$ ]
MM499	0.853 [0.807-1.287]	0.813 [0.539-0.859]	0.089 [0.083-0.100]	7.753 [6.931-8.402]
MM528	0.707 [0.661-0.746]	0.980 [0.929-1.049]	0.061 [0.045-0.070]	11.44 [9.846-15.44]
MM530	0.523 [0.372-0.575]	1.325 [1.205-1.863]	0.053 [0.035-0.064]	13.00 [10.85-19.86]
Mean	0.645	1.130	0.058	14.24
S.D.	0.168	0.279	0.025	7.351

<sup>a</sup>Values in parentheses represent the lower and upper 68% confidence intervals, calculated by a bootstrap method in which each experiment was simulated 1000 times.

**Table 3.** Plasma viral loads of selected samples measured by RT-PCR with a lower detection limit (20 copies/ml) in group A animals during cART.

Animals ID	Plasma viral loads (copies/ml)			
	29wpi	42wpi	52wpi	At autopsy <sup>a</sup>
MM491	< 20	< 20	< 20	< 20
MM499	< 20	< 20	< 20	< 20
MM528	< 20	< 20	< 20	< 20
MM530	< 20	44	47	< 20

<sup>a</sup>MM491, 63 wpi; MM499, 64 wpi; MM528, 61 wpi; MM530, 65 wpi.

**Table 4.** Antiretroviral activities detected in the blood of animals in group A during cART.

Animals ID	Drug concentration ( $\mu\text{M}$ ) <sup>a</sup>					
	10wpi	20wpi	32wpi	42wpi	56wpi	At autopsy <sup>b</sup>
MM491	3.5	15.9	12.1	17.8	7.9	5.2
MM499	0.6	2.3	4.4	11.4	1.7	0.9
MM528	16.0	24.9	6.6	7.7	6.0	9.3
MM530	9.4	12.4	8.2	14.2	11.3	11.3

<sup>a</sup>LPV/RTV equivalent concentration.

<sup>b</sup>MM491, 63 wpi; MM499, 64 wpi; MM528, 61 wpi; MM530, 65 wpi.

Table 5

**Table 5.** Viral RNA burdens in various tissues collected from SIV-infected macaques.

Tissues	vRNA levels (copies/ $\mu$ g total RNA)				
	treated with cART				untreated
	MM491	MM499	MM528	MM530	MM521
	<200 copies/ml <sup>a</sup>	<200 copies/ml <sup>a</sup>	<200 copies/ml <sup>a</sup>	<200 copies/ml <sup>a</sup>	1.2 $\times$ 10 <sup>6</sup> copies/ml <sup>a</sup>
Non-lymphoid tissues					
heart	<2900	<2900	<2900	<2900	3.0 $\times$ 10 <sup>3</sup>
liver	<2900	<2900	<2900	<2900	8.8 $\times$ 10 <sup>4</sup>
kidney	<2900	<2900	<2900	<2900	2.1 $\times$ 10 <sup>6</sup>
CNS tissues					
cerebrum	<2900	<2900	<2900	<2900	1.1 $\times$ 10 <sup>6</sup>
cerebellum	<2900	<2900	<2900	<2900	4.5 $\times$ 10 <sup>3</sup>
brain stem	<2900	<2900	<2900	<2900	<2900
Effector sites					
lung	4.7 $\times$ 10 <sup>3</sup>	4.1 $\times$ 10 <sup>3</sup>	<2900	<2900	1.0 $\times$ 10 <sup>5</sup>
vagina	6.5 $\times$ 10 <sup>3</sup>	<2900	<2900	2.9 $\times$ 10 <sup>3</sup>	1.3 $\times$ 10 <sup>5</sup>
jejunum	5.0 $\times$ 10 <sup>3</sup>	3.1 $\times$ 10 <sup>3</sup>	1.1 $\times$ 10 <sup>4</sup>	7.4 $\times$ 10 <sup>3</sup>	1.7 $\times$ 10 <sup>6</sup>
ileum	5.2 $\times$ 10 <sup>3</sup>	4.0 $\times$ 10 <sup>3</sup>	7.7 $\times$ 10 <sup>3</sup>	<2900	1.4 $\times$ 10 <sup>6</sup>
colon	1.8 $\times$ 10 <sup>4</sup>	<2900	6.5 $\times$ 10 <sup>4</sup>	8.3 $\times$ 10 <sup>3</sup>	2.0 $\times$ 10 <sup>8</sup>
rectum	2.9 $\times$ 10 <sup>3</sup>	<2900	6.0 $\times$ 10 <sup>3</sup>	9.9 $\times$ 10 <sup>3</sup>	4.7 $\times$ 10 <sup>6</sup>
Lymphoid tissues					
spleen	2.6 $\times$ 10 <sup>4</sup>	5.0 $\times$ 10 <sup>3</sup>	5.4 $\times$ 10 <sup>3</sup>	6.2 $\times$ 10 <sup>3</sup>	3.4 $\times$ 10 <sup>8</sup>
thymus	<2900	<2900	N.D.	2.0 $\times$ 10 <sup>5</sup>	2.9 $\times$ 10 <sup>4</sup>
iliac LN	5.8 $\times$ 10 <sup>4</sup>	6.9 $\times$ 10 <sup>3</sup>	1.5 $\times$ 10 <sup>4</sup>	3.6 $\times$ 10 <sup>4</sup>	1.6 $\times$ 10 <sup>8</sup>
inguinal LN	<2900	2.4 $\times$ 10 <sup>4</sup>	2.4 $\times$ 10 <sup>4</sup>	2.3 $\times$ 10 <sup>5</sup>	6.9 $\times$ 10 <sup>7</sup>
axillary LN	8.6 $\times$ 10 <sup>4</sup>	7.2 $\times$ 10 <sup>3</sup>	3.1 $\times$ 10 <sup>4</sup>	2.1 $\times$ 10 <sup>5</sup>	7.6 $\times$ 10 <sup>7</sup>
iMLN	1.0 $\times$ 10 <sup>5</sup>	8.8 $\times$ 10 <sup>4</sup>	<2900	2.9 $\times$ 10 <sup>5</sup>	1.0 $\times$ 10 <sup>8</sup>
sMLN	1.3 $\times$ 10 <sup>5</sup>	5.7 $\times$ 10 <sup>4</sup>	3.4 $\times$ 10 <sup>4</sup>	2.4 $\times$ 10 <sup>5</sup>	2.3 $\times$ 10 <sup>8</sup>
submandibular LN	6.2 $\times$ 10 <sup>4</sup>	2.9 $\times$ 10 <sup>4</sup>	1.6 $\times$ 10 <sup>4</sup>	5.6 $\times$ 10 <sup>3</sup>	3.9 $\times$ 10 <sup>7</sup>
bronchial LN	1.5 $\times$ 10 <sup>5</sup>	5.3 $\times$ 10 <sup>4</sup>	3.1 $\times$ 10 <sup>4</sup>	3.8 $\times$ 10 <sup>5</sup>	1.1 $\times$ 10 <sup>8</sup>
splenic LN	2.5 $\times$ 10 <sup>5</sup>	4.3 $\times$ 10 <sup>4</sup>	7.3 $\times$ 10 <sup>3</sup>	2.0 $\times$ 10 <sup>5</sup>	9.8 $\times$ 10 <sup>7</sup>

N.D., no data; CNS, central nervous system; LNs, lymph nodes; iMLNs, inferior mesenteric lymph nodes; sMLNs, superior mesenteric lymph nodes.

Viral RNA levels (copies/ $\mu$ g total RNA) are coded in grayscale as follows: white boxes, <2900; light-gray boxes, <1.0 $\times$ 10<sup>5</sup>; dark-gray boxes, <1.0 $\times$ 10<sup>7</sup>; black boxes, >1.0 $\times$ 10<sup>7</sup>.

<sup>a</sup>Viral loads in plasma.

**Table 6.** Viral loads in plasma samples of animals in group B.

Animal ID	plasma viral loads (copies/ml)					
	0wpi	2wpi	8wpi	38wpi	46wpi	At autopsy <sup>a</sup>
MM508	<200	$8.4 \times 10^6$	$2.6 \times 10^5$	$3.8 \times 10^4$	<200	<200
MM511	<200	$7.7 \times 10^6$	$3.1 \times 10^5$	$1.1 \times 10^5$	<200	$1.4 \times 10^3$

The animals were treated with cART from 38 wpi to 46 wpi.

<sup>a</sup>47.5 wpi

**Table 7.** Viral RNA burdens in various tissues collected from animals in group B.

Tissues	vRNA levels (copies/ $\mu\text{g}$ total RNA)	
	MM508	MM511
	PVL, <200 copies/ml	PVL, 1400 copies/ml
Non-lymphoid tissues		
heart	<2900	<2900
liver	<2900	<2900
kidney	<2900	<2900
CNS tissues		
cerebrum	<2900	<2900
cerebellum	<2900	<2900
brain stem	<2900	<2900
Effector sites		
lung	<2900	<2900
vagina	<2900	N.D.
upper intestinal tract	<2900	<2900
lower intestinal tract	<2900	<2900
Lymphoid tissues		
spleen	<b><math>2.0 \times 10^5</math></b>	<b><math>7.4 \times 10^5</math></b>
thymus	<2900	<2900
iliac LN	<b><math>1.4 \times 10^4</math></b>	<b><math>3.5 \times 10^5</math></b>
inguinal LN	<2900	<b><math>5.3 \times 10^5</math></b>
axillary LN	<b><math>1.9 \times 10^4</math></b>	<b><math>1.3 \times 10^6</math></b>
iMLN	<b><math>1.3 \times 10^5</math></b>	<b><math>1.6 \times 10^6</math></b>
sMLN	<b><math>8.4 \times 10^3</math></b>	<b><math>1.5 \times 10^6</math></b>
submandibular LN	<b><math>1.1 \times 10^5</math></b>	<b><math>9.4 \times 10^5</math></b>
bronchial LN	<b><math>1.1 \times 10^4</math></b>	<b><math>9.5 \times 10^5</math></b>
splenic LN	<b><math>9.9 \times 10^4</math></b>	N.D.

PVL, plasma virus load; N.D., no data; CNS, central nervous system; LNs, lymph nodes; iMLNs, inferior mesenteric lymph nodes; sMLNs, superior mesenteric lymph nodes.

Viral RNA levels (copies/ $\mu\text{g}$  total RNA) are colored in grayscale as follows: white boxes, <2900; light-gray boxes,  $<1.0 \times 10^5$ ; dark-gray boxes,  $<1.0 \times 10^7$ .

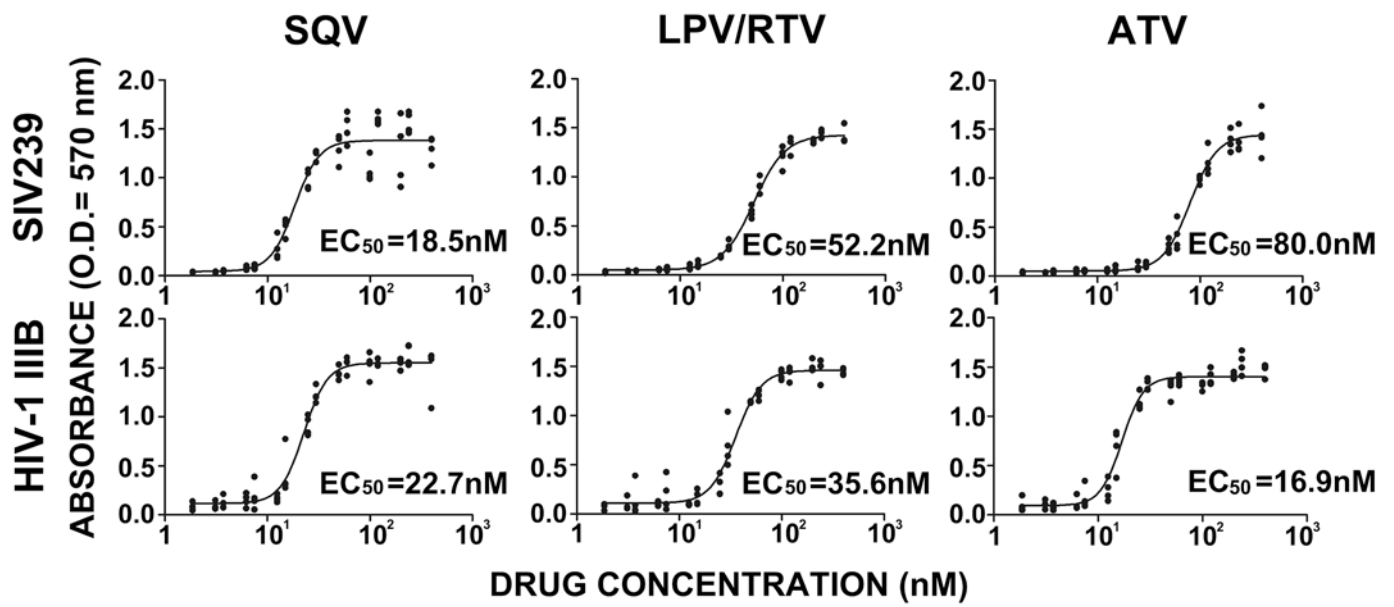


**Table 8.** Numbers of immunohistochemistry sections examined from macaques in group B.

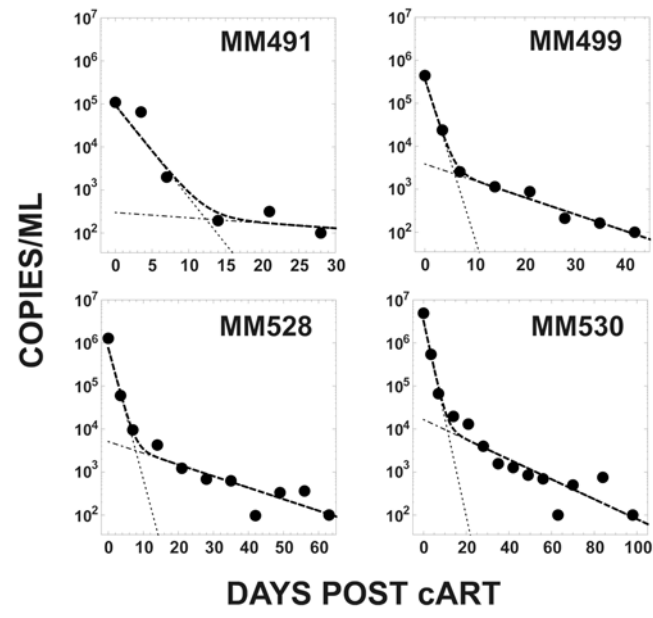
Nef expressing T cells	Number of sections subjected				total
	MM508		MM511		
	MLN	Non-MLN	MLN	Non-MLN	
present in the follicles	0	0	9	3	12
present in the paracortical area	1	0	3	1	5
absent	50	85	34	255	424

MLNs; mesenteric lymph nodes.

Supplementary Figure 1.



Supplementary Figure 2.



Supplementary Figure 3.

